CHALMERS

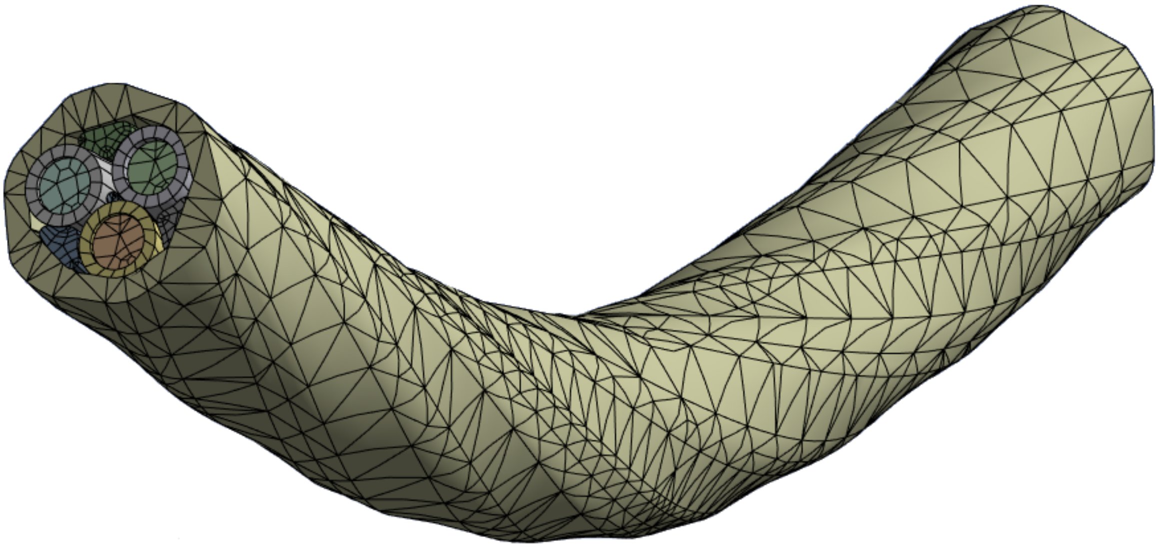

Finite element modelling of dynamic power cable for marine renewable installations

Examensarbete inom högskoleprogrammet, Maskinteknik

Emil Hammar
Axel Waszkiewicz

INSITUTIONEN FÖR MEKANIK OCH MARITIMA VETENSKAPER

CHALMERS TEKNISKA HÖGSKOLA

Göteborg, Sverige 2025
www.chalmers.se

Examensarbete 2025

Finite element modelling of dynamic power cable for marine renewable installations

EMIL HAMMAR
AXEL WASZKIEWICZ

Institutionen för Mekanik och Maritima Vetenskaper
CHALMERS TEKNISKA HÖGSKOLA
Göteborg, Sverige 2025

Finite element modelling of dynamic power cable
for marine renewable installations

EMIL HAMMAR
AXEL WASZKIEWICZ

Examiner/Supervisor: Zhiyuan Li, Department of Mechanics and Maritime Sciences, Chalmers University of Technology

Examensarbete MMSX25

Institutionen för Mekanik och Maritima vetenskaper

Chalmers tekniska högskola

412 96 Göteborg, Sverige

Telefon: + 46 (0)31-772 1000

Omslagsbild: 3D modell baserat på en kabel från Chalmers. Bild tagen av Emil Hammar via Ansys Mechanical.

Finite element modelling of dynamic power cable for marine renewable installations

EMIL HAMMAR
AXEL WASZKIEWICZ

Department of Mechanics and Maritime Sciences
Chalmers University of Technology
Gothenburg, Sweden, 2025

Abstract

The purpose of this study is to analyze and further develop a marine power cable by combining mechanical, electrical, and thermal simulations with previous experimental data from a tested cable. The project is based on an existing cable that has been subjected to tensile, bending, torsion, and fatigue testing at the Department of Mechanics and Maritime Sciences at Chalmers University of Technology. By digitally modelling the cable’s cross-section and lay length in CAD software (Fusion 360) and conducting finite element simulations in ANSYS Workbench, the behavior of the cable under various loading conditions can be analyzed with high accuracy.

A central objective is to investigate how to replicate an experiment to a digital analysis by using FEA, particularly in bending and tension. In parallel, the study also includes an analysis of the cable's electrical and thermal behavior, focusing on how heat is generated in the conductor and transferred through the insulation layers with a simplified cable model. This is being done to provide a comprehensive understanding of the cable’s performance under realistic operational conditions with a simpler model without the need for extensive computer power that is not available for the average person.

Because fiber-based conductor materials, such as helically winded copper wires, lead to nonlinear models that are computationally heavy, the study purposefully includes calculations of effective material properties and analysis of different moments of inertias. This allows simplification of geometry by modelling fiber bundles as solid bodies with equivalent mechanical behavior, significantly reducing simulation time without sacrificing accuracy.

The goal is to compare the simulation results with previous experimental data to validate the model and use it as a foundation for improving the cable’s design in future studies. These improvements may include new material choices, modified geometry, or new combinations of structural layers. The overall objective is to develop a cable that can be stronger, lighter, and more reliable. Additionally, the cable should be easier to handle during maintenance and better suited for use in marine environments, both in terms of electrical efficiency and mechanical durability.

This report is written in English.

Finite element modelling of dynamic power cable for marine renewable installations
EMIL HAMMAR
AXEL WASZKIEWICZ

Institutionen för Mekanik och Maritima vetenskaper
Chalmers tekniska högskola
Göteborg, Sverige, 2025

Sammanfattning

Syftet med denna studie är att analysera och vidareutveckla en marin kraftkabel genom att kombinera mekaniska, elektriska och termiska simuleringar med tidigare experimentella data från en testad kabel. Projektet bygger på en befintlig kabel som har genomgått drag-, böj-, vridnings- och utmattningsprovningar vid Institutionen för Mekanik och Maritima Vetenskaper vid Chalmers tekniska högskola. Genom att digitalt modellera kabelns tvärsnitt och slaglängd i CAD-programvara (Fusion 360) samt genomföra finita element-simuleringar i ANSYS Workbench kan kabelns beteende under olika belastningsförhållanden analyseras med hög noggrannhet.

Ett centralt mål är att undersöka hur ett experiment kan återskapas i en digital analys med hjälp av finita elementmetoden (FEM), särskilt för böjning och dragbelastning. Parallellt omfattar studien även en analys av kabelns elektriska och termiska egenskaper, med fokus på hur värme genereras i ledaren och transporteras genom isoleringslagren med hjälp av en förenklad kabelmodell. Detta görs för att ge en heltäckande förståelse av kabelns prestanda under realistiska driftförhållanden med en enklare modell, utan behov av omfattande datorkraft som normalt inte är tillgänglig för gemene användare.

Eftersom fiberbaserade ledarmaterial, såsom helikalt tvinnade koppartrådar, leder till olinjära modeller som är beräkningsmässigt krävande, inkluderar studien medvetet beräkningar av effektiva materialegenskaper samt analyser av olika tröghetsmoment. Detta möjliggör förenkling av geometrin genom att modellera fiberbuntarna som solida kroppar med ekvivalent mekaniskt beteende, vilket avsevärt minskar simuleringstiden utan att kompromissa med noggrannheten.

Målet är att jämföra simuleringsresultaten med tidigare experimentella data för att validera modellen och använda den som grund för att förbättra kabelns konstruktion i framtida studier. Dessa förbättringar kan omfatta nya materialval, modifierad geometri eller nya kombinationer av strukturella lager. Det övergripande syftet är att utveckla en kabel som är starkare, lättare och mer tillförlitlig. Dessutom ska kabeln vara enklare att hantera vid underhåll och bättre lämpad för användning i marina miljöer, både ur ett elektriskt effektivitets- och mekaniskt hållbarhetsperspektiv.

Denna rapport är skriven på engelska.

Contents

List of Tables

List of Figures

1. Introduction

As the push for offshore renewable energy continues to grow, the role of marine power cables has become more important than ever. These cables are used to connect floating energy systems like offshore wind turbines and wave energy converters to the grid. But in these harsh environments, it’s not just about getting electricity from point A to point B. The cables must survive constant motion, changing loads, and tough underwater conditions over many years.

One of the biggest challenges is making sure the cable can handle both the heat generated by electrical current and the mechanical forces it will experience in the ocean. On the thermal side, when electricity flows through the copper conductor, it creates heat. If that heat isn’t managed properly, it can build up and push the cable materials past safe temperature limits.

At the same time, repeated bending, twisting, and tension from floating systems can over time wear down the materials, cause fatigue, and eventually lead to failure. That is why understanding the mechanical properties of the cable, like its flexibility, stiffness, and how its layers interact is vital to predict long-term reliability.

This project not only addresses technical challenges but also contributes to global sustainability goals by enabling reliable offshore renewable energy systems. Due to time constraints, the project focuses on modeling and simulating a 1 kV marine power cable using CAD and FEA tools. The scope includes steady-state and transient thermal simulations, bending and tension analysis, and comparison with previous experimental data. Torsion and fatigue simulations are excluded. Simplifications were necessary to keep the model practical, such as representing the helically wound conductor as a solid cylinder in thermal analysis and assuming a fixed seawater temperature of 2 °C [1]. Frictional contact between layers and dynamic electrical resistivity changes were approximated and not fully modeled.

Previous research supports the approach used in this study. Ma et al. [2] highlighted the importance of accurate convection modeling for submarine cables, while González-Cagigal et al. [3] validated electro-thermal models against real measurements. Del-Pino-López et al. [4] demonstrated that geometric and material simplifications are essential for computational efficiency in FEM simulations. These studies confirm that the methods adopted here, i.e. explicit convection calculation, validated electro-thermal modeling principles, and controlled simplifications are consistent with best practices. By combining thermal and mechanical analysis, this study aims to understand how the cable will perform in real marine conditions and ensure it remains safe, reliable, and durable. Thus, it can keep doing its job without failure, even in some of the most demanding environments on the planet, the sea. Furthermore, by improving the reliability and efficiency of subsea power cables, projects can improve the infrastructure needed for large-scale renewable energy deployment. These technologies support offshore renewable energy systems, such as wind and wave power, and contribute directly to the United Nations' 2030 Agenda for Sustainable Development. Especially two goals from the sustainable development agenda.

Goal 13: Climate Action, by reducing greenhouse gas emissions and mitigating climate change through the transition to renewable energy. [5]

Goal 7: Affordable and Clean Energy, by providing access to reliable, modern, and sustainable energy sources. [6]

2. Methodology

This chapter explores key preparations and acknowledgment to inspect with the utilization of FEA software. Many subchapters recognize general knowledge that is to be considered into thought for analyzing the results.

2.1 Modelling the cable

The cable model is based on an experiment that was done by Chalmers University and other collaborative hosts [7]. It is a marine power cable mainly for water energy converters (WEC) and has been researched for a more robust, user friendly and simpler maintenance operation, without heavy reparation costs long term [8]. The report provides geometry measurement and a cross-sectional area to base a sketch with the software Autodesk Fusion 360. Another report from Chalmers University has been used for further geometry measurements, particularly the area for the aramid fiber [8]. The table below summarizes the key geometry measurements.

Table 1: Key geometry values for modelling [7, 8]

Cable Component	1kV	3,6kV
Copper Conductor diameter (mm)	9,3	9,3
Conductor insulation thickness (mm)	2	2,5
Outer diameter (mm)	38	39,7
Lay Length (mm)	300-600 (median = 450)	400-800 (median = 600)
Kevlar diameter (mm)	6,4	-
Optic fiber (mm)	1	-

The available results from reference [7] show specifically from a 3,6kV cable. However, the dimensions from the 1kV and 3,6 kV models are very similar. The simulation results for a 1kV and 3,6kV would be quite similar. This research will therefore focus on the 1kV, compare its FEA results with the previous report and discuss the accuracy. Using Fusion's circular pattern tools, the components can efficiently be implemented in a 2D sketch.

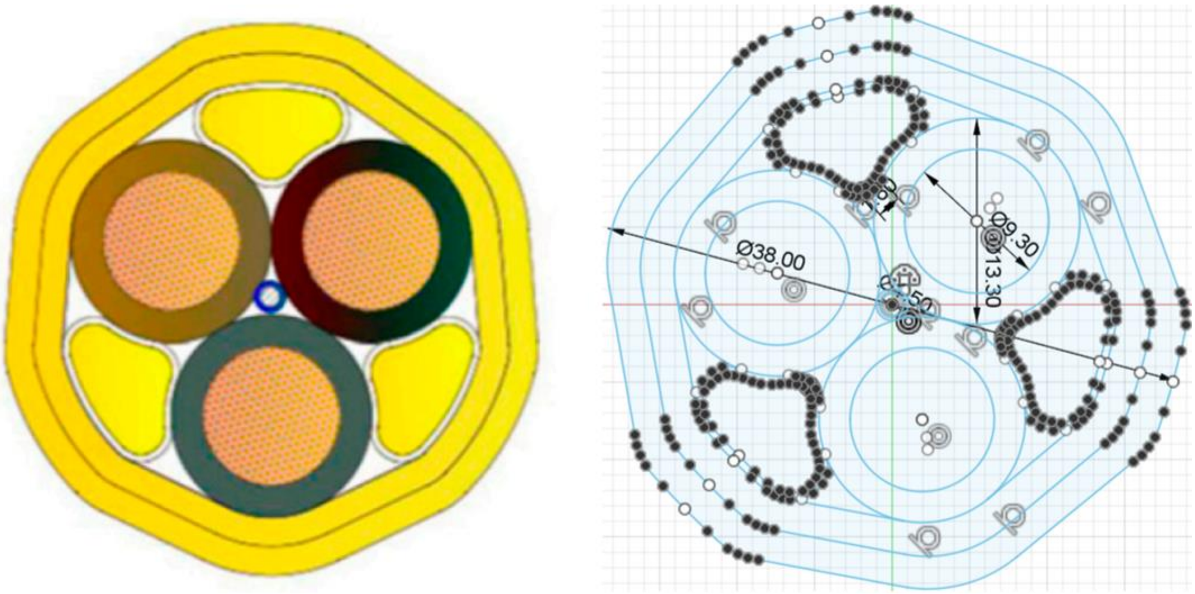

Figure 1: Base model from [7] and the sketch models from Fusion 360

The 2D sketch can furthermore be extruded into a 3D body. To include helical winding, the 2D sketch can be marked for Fusion's sweep tool. This allows the body to twist the desired rotation depending on the desired length. The sweep tool is executed with the key lay length according to Table 1.

Figure 2: First draft extruded cable with desired twist in Fusion 360

For FEA utilization, the outer shells can be fused into one body. This will minimize the number of nodes and elements while generating mesh. Less number of nodes and elements will result in faster solving time, due to less calculations. The outer shells are made of TPU and typically have very high friction coefficient depending on their hardness [9-12]. In addition, the shells around every aramid fiber and optic fiber body can be removed in the modeling, due to them being very thin. Thin layers often cause meshing instability and increase computational cost in FEA. This approach is supported by Del-Pino-López et al. [4], who concluded that geometric simplifications are necessary for convergence and efficiency in cable FEM analysis.

For this cable model, surface contact could be generated through thin bodies as such for the aramid fiber shells. As an example, Kevlar could have a generated contact region with XLPE insulation through the aramid fiber shell. This could make the simulation unstable and increase the solving time significantly. Furthermore, thin bodies require more nodes and elements for their mesh to be successfully generated, which will increase solving time even more. The study will furthermore include models with one-dimensional beam elements which can be generated with ANSYS SpaceClaim. The figure below visualizes the finalized version with the correct area of aramid fiber, fused outer shells, removed shells for optic fiber and aramid fiber, and a model with line bodies as conductors.

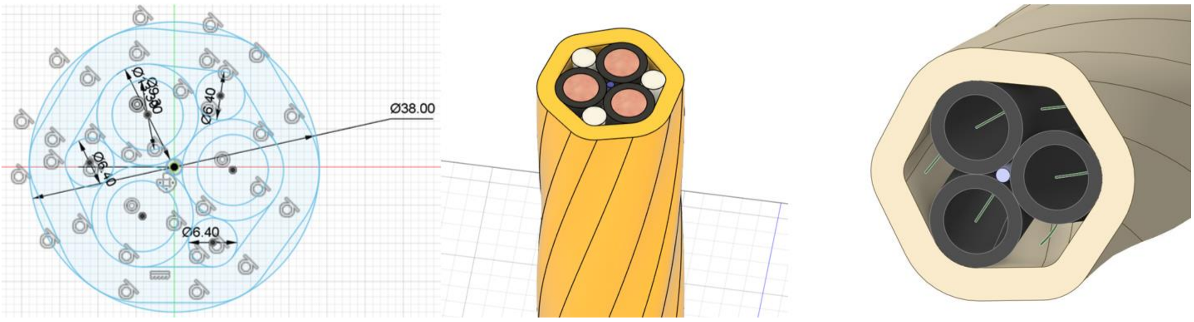

Figure 3: Finalized models for FEA software

The study will furthermore focus on the conductors for increased understanding in boundary conditions for contact applications between a solid element and a beam element. The beam element in FEA software allows user-defined properties in its cross-section. This allows for customized properties like the area moment of inertia that is usually automatically generated from the geometric model. Automatically generated properties, from a modeled geometry, that are altered are considered “user-defined” in the Ansys Mechanical software. The conductors will be analyzed on three different occasions. One single conductor, one straight triple conductor and one helically winded triple conductor. The dimensions are all the same as the 1kV cable, including conductor bundle diameter and insulation thickness.

Figure 4: Conductor models

2.2 Material properties

Accurate representation of material behavior is important for ensuring the reliability of multi-physics simulations, especially when analyzing the electro-thermal and mechanical performance of marine cables. The cable model used in this study consists of four main layers, each chosen for its specific electrical, thermal, or mechanical function in demanding underwater environments. These materials include pure copper as the conducting core, cross-linked polyethylene (XLPE) as the primary electrical insulation, a combination of Kevlar 29 and Kevlar 49 as the mechanical reinforcement layer, and thermoplastic polyurethane (TPU) as the outer protective sheath [7]. The original cable design from Chalmers also contains an optical fiber [7]. For simplicity, most analyses will exclude the optical fiber's influence on the overall performance, although its material properties are still considered to maintain accuracy. The lack of influence on the overall performance would only increase unnecessary time consumption for the solver. The material is usually silica based or an acrylic based material [13]. Fused silica was chosen for some of the simulations.

Material data for all five components were available from the ANSYS Granta EduPack Level 3 database [14]. Level 3 database is an advanced and broad collection of data for individual material properties and its manufacturing capabilities. Median property values were used consistently in both analytical calculations and finite element simulations (FEA) to keep the mechanical, electrical, and thermal models as realistic as possible. There is identical Copper (C10100) that is either soft or hard. Both are pure but have been treated differently. Thus, resulting in different properties. Previous experiments [7, 8] did not specify the treatment of the utilized Copper which led to using both for comparison.

Table 2: Material property of 4/5 components [14]

	Copper (C10100) soft	Copper (C10100) hard	XLPE	TPU (Polyurethane)	Silica (fused)
Density (kg/m^3)	8940 - 8960	8940 - 8960	920 - 1240	1120 - 1220	2170 - 2220
Young's Modulus (GPa)	122 - 128	125 - 135	0,537 - 0,56	0,0197 - 0,275	71,2 - 74,8
Poisson's Ratio	0,34 - 0,35	0,34 - 0,35	0,431 - 0,433	0,48 - 0,495	0,15 - 0,16
Tensile Yield Strength (MPa)	50 - 70	185 - 340	14 - 23	29,5 - 37,5	152 - 168
Compressive Yield Strength (MPa)	50 - 70	185 - 340	9,92 - 16,6	35,4 - 45	1520 - 1680
Shear modulus (GPa)	44 - 46	45 - 50	0,188 - 197	0,00659 - 0,00929	30,8 - 32,3
Thermal Conductivity (W/m·K)	390 - 398	390 - 398	0,175 – 0,182	0,133 - 0,15	1,2 - 1,5
Coefficient of Thermal Expansion (K^{-1})	$(16,8 - 17,3) \cdot 10^{-6}$	$(16,8 - 17,3) \cdot 10^{-6}$	$(176 – 184) \cdot 10^{-6}$	$(160 – 170) \cdot 10^{-6}$	$(0,51 - 0,55) \cdot 10^{-6}$
Max Continuous Operating Temperature (°C)	77 - 87	77 - 87	90 - 110	93 - 107	900 - 1100
Specific heat (J/kg·°C)	383 - 387	383 - 387	1600 - 1670	1550 - 1640	700 - 750
Electrical Resistivity (Ωm)	$(1,7 - 1,74) \cdot 10^{-8}$	$(1,7 - 1,74) \cdot 10^{-8}$	$2,37 \cdot 10^{15}$ - $2,13 \cdot 10^{16}$	$2,5 \cdot 10^{9}$ - $1,8 \cdot 10^{10}$	10^{15} - 10^{17}

Kevlar uses the Young modulus of 110 GPa [7] which does not exist in the Granta Edupack database. Three variants are available and are most likely mixed with Kevlar 29 and Kevlar 49. This can be numerically calculated using Python with the Rule of Mixture (ROM) formula.

$$E_{eff} = V_1 \cdot E_1 + V_2 \cdot E_2 \tag{1}$$

(E_i) is the young modulus of each material and (V_i) between 0-1 is the volume factor of each material. The results show a volume mixture of 0,339 of Kevlar 29 and 0,661 of Kevlar 49 with the median elasticity value. 71 GPa and 130 GPa from Kevlar 29 and 49. Please see Appendix A for fully detailed Python script. Rule of mixture (ROM) or Voight iso-strain averaging is a method to average the mechanical structure between materials into their effective property (E_{eff}). This method can be used if the materials are assumed to have equal strain [15]. For simplicity in this study, the averaging was used for every other property of Kevlar 29 and 49 disregarding any slip between the fibers. Table 3 displays the effective properties of the Kevlar mixture.

Table 3: General and effective material property for 1/5 components [14]

	Kevlar 29	Kevlar 49	0,339 Kevlar 29 & 0,661 Kevlar 49 Mixture
Density (kg/m³)	1430 - 1450	1440 - 1450	1 436,61 - 1450
Young's Modulus (GPa)	62 - 80	125 - 135	103,643 - 116,335
Poisson's Ratio	0,35 - 0,37	0,35 - 0,36	0,35 - 0,36339
Tensile Yield Strength (MPa)	2500 - 3000	2250 - 2750	2 334,75 - 2 834,75
Compressive Yield Strength (MPa)	200 - 300	200 - 300	200 - 300
Shear modulus (GPa)	1 - 1,3	1 - 1,3	1 - 1,3
Thermal Conductivity (W/m·K)	0,2 - 0,3	0,2 - 0,3	0,2 - 0,3
Coefficient of Thermal Expansion (K^{-1})	(-3,4) - (-3,2)	(-4) - (-2)	(-3,7966) - (-2,4068)
Max Continuous Operating Temperature (°C)	200 - 300	200 - 300	200 - 300
Specific heat (J/kg·°C)	1350 - 1450	1350 - 1450	1350 - 1450
Electrical Resistivity (Ωm)	10^{11} - 10^{15}	10^{11} - 10^{15}	10^{11} - 10^{15}

The thermal elasticity can be included. Granta Edupack has data for copper and XLPE. This is particularly interesting when the displacement and eventual stress is affected by heat transferred inside the cable.

Table 4: Thermal elasticity C10100 hard [14]

Temperature (°C)	Elasticity (GPa)
-200	136
-100	133
0	128
100	122
200	116
300	110
400	104
500	97
600	90
700	84
800	76
900	68
1000	60

Table 5: Thermal elasticity XLPE [14]

Temperature (°C)	Elasticity (GPa)
20	0,56
30	0,46
40	0,38
50	0,31
60	0,25
70	0,19
80	0,15
90	0,12
100	0,09
110	0,07

All necessary material properties, depending on the simulation focus, could be implemented in Ansys Workbench’s Engineering data. It could be implemented by assigning new custom material and picking the necessary properties from the toolbox, please see the figure below.

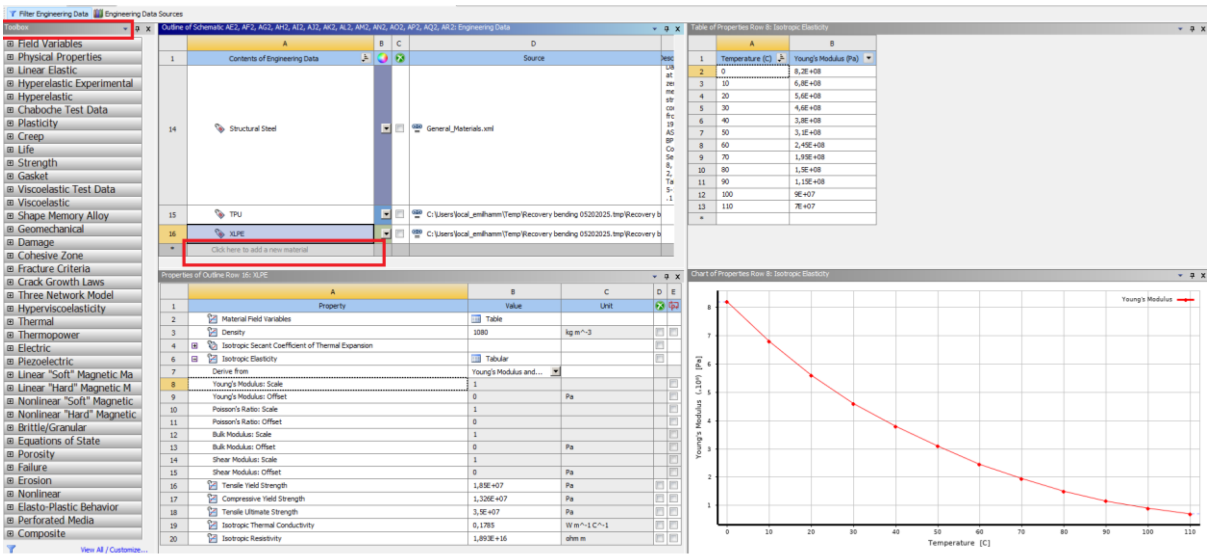

Figure 5: Ansys Workbench’s Engineering data with materials, example XLPE

2.3 Electric thermal conversion

The electric–thermal analysis of the marine cable was carried out to study how the electrical current affects the thermal state of the cable and how the cables’ long-term reliability is impacted. When current flows through the conductor with resistance, the resistive losses generate heat so called joule heating, which must dissipate to avoid the material degrading. If heat accumulates, insulation layers such as XLPE might exceed temperature limits while mechanical strength and aging of the cable will follow.

The analysis combined electrical and thermal physics, focusing on how resistance in the conductor creates heat and how that heat is transferred through and away from the system. A combination of analytical calculations and finite element simulations was used in ANSYS Workbench to perform the study.

The analysis combines three major principles. Joule Heating, the heat generation due to electrical resistance in the conductor. Heat Conduction, the transfer of heat through the cable layers (copper, XLPE, Kevlar, TPU) according to Fourier's law. Lastly, Convective Cooling, the heat removal from the cable surface to seawater using Newton's law of cooling. Radiative heat transfer is neglected because it is not significant at the operating temperature of marine cables.

The model uses simplified geometry (conductor as a solid cylinder instead of multiple individual fibers) to reduce computational effort while retaining essential accuracy [4]. The goal is to predict temperature distribution under realistic offshore conditions and ensure thermal safety margins for continuous operation.

2.4 Effective material properties

A solid core copper conductor behaves differently from a fiber bundle conductor of the same volume. The reason for this is that bending stiffness depends on flexural rigidity, the product of elasticity and area moment of inertia (E · I). A solid core has a much higher (I) which makes it stiffer. A stranded conductors can have movement between fibers which reduces effective stiffness and increase flexibility. A copper conductor based on fibers is much more flexible in bending and torsion depending on how the fibers are layered out. As for tension, that can be approximately the same as a solid core depending on how much volume corresponding to the solid core it is using. Meaning that both elasticity and area moment of inertia are altered for it to behave differently in displacement and strength.

In theory, this could be converted into a composite material where at least two materials combine into a third material on a macroscopic scale. There are different classifications that can be accepted as composite material. Common classification that resembles copper fibers in a cable, is "Fibrous composite materials that consist of fibers in a matrix" [16]. Composite material in general has been a method to reinforce applications by combining one or more of these broad categories: metals, ceramics, and polymers. Throughout history, this has resulted in high-stiffness, high-strength and low-density for various applications like aircraft, automotive, marine, energy, infrastructure, armor, biomedical and recreational (sports) applications [17]. This composite theory cannot be fulfilled due to no second solid material present in the fiber bundles. There are either voids of air or lube inside the bundles. Both elements are not solid and cannot follow for the composite theory. Some structure elements like helical winding are of use for this study.

This section will mainly focus on volume mixture and on helical winding structure. Furthermore, there are a few formulas of area moment of inertia that in turn represent different states of interactions between the fibers.

2.4.1 Volume mixture

The volume factor is crucial for theoretically calculating the effective properties in composite materials. For this research, using a 2D hexagonal shape is the tightest packing that is achievable. The formula for the volume factor can be retrieved from copper and Kevlar [18, 19].

$$\eta_{Cu} = V_f = \frac{\pi}{2 \cdot \sqrt{3}} = 0{,}906899\ldots \approx 0{,}907 \tag{2}$$

This formula assumes that all circles are tightly packed together, furthermore with the outer layer. Signifying that there are no big empty areas between each circle and outer boundary. This theorem includes no overlapping furthermore [19]. This can be further accurate with a python script to generate fibers and fit within a cylinder in a 2D hexagonal shape. Resulting in an accurate number of fiber and volume factors. The script displays each fiber in a coordinate system that is tightly fit inside the inner radius of the insulation. This script includes the center of fibers just by the inner radius, resulting in eventual compressive force within the fibers. In practicality, conductors in this fit would be stiffer. This will result in another volume factor compared to equation (2) that does not include any overlapping to the outer boundary, please see Figure 6. The fiber diameter for copper is approximately 0,31 mm according to the IEC standards [20]. The fiber diameter for Kevlar is approximately 0,015 mm [14]. Please see Appendix C for the full script. The thickness of the fiber could explain the difference from

Figure 6. The copper fibers are approximately 20 times thicker than Kevlar fibers and could explain that the thicker the fibers the more likely they are to overlap with the outer boundary.

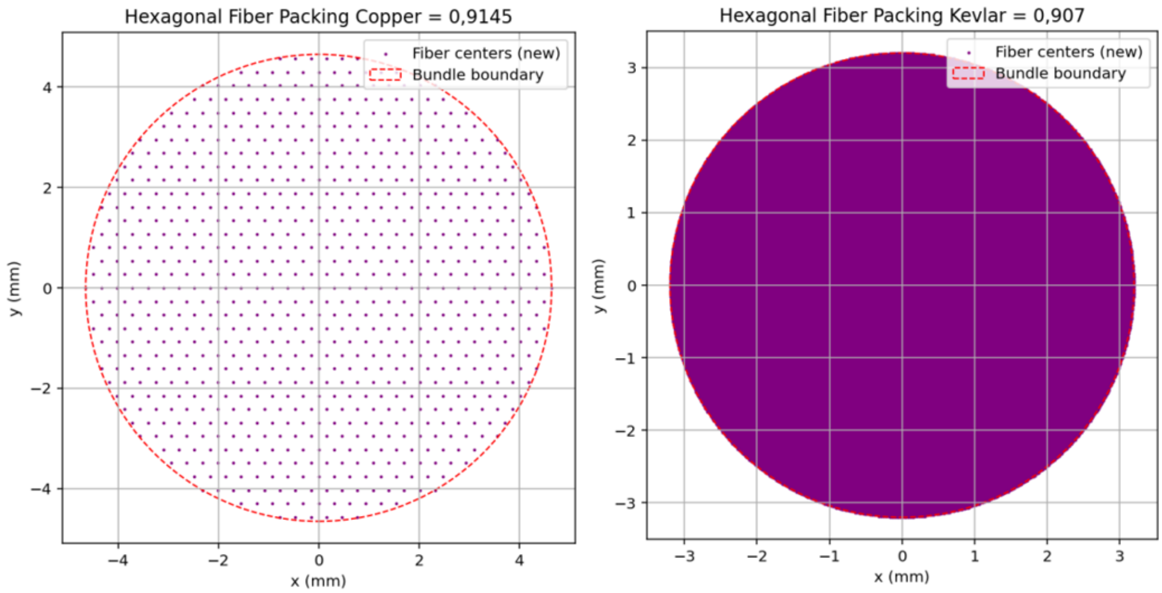

Figure 6: Visualization of fiber placement for Copper and Kevlar

2.4.2 Helical Winding

With a Python script, the formulas of composite mechanics regarding helical winding and property values from volume mixture can be implemented. The properties of copper fibers and Kevlar can be automatically calculated. Appendix B shows the script in full detail. Adding a geometric winding would need a very fine mesh and other complex settings, which would take a lot of time and computer power. Using a straight and solid shape instead would give the results that are good enough for this study and keep the project practical. Helical winding is a particular structure that is used for a material's anisotropic behavior. This study will utilize the equations for helical winding and analyze its influence. The equations use existing parameters to transform its elasticity matrix. The properties of helical winding depend on the lay angle of the fibers and are usually not the same in each layer. The lay angle can be from 0-15 degrees depending on each layer [21]. Formulas can further transform a unidirectional fiber composite according to reference [16]. However, only a singular lay angle can be used, unless the volume factor is divided into each fiber layer. Therefore, the lay angle has been set to 10 degrees as average.

The equation is a continuation of Hooke's law that includes the matrix [T] to transform the fibers elasticity from their local coordinates to the bundle's local coordinate. The fibers local coordinate system is interpreted as numbers (1, 2, 3) instead of the bundle's axis (x, y, z) The modulus used by Hooke's law furthermore utilizes their engineering constants (S_{ij}) for anisotropic compliance. The equations are simplified as fibers local coordinates 2 and 3 are similar in property. This is similar for planes 12 and 13. Furthermore with the bundle's transverse coordinate system. Only the plane (G_{yz}) remains unaffected. [16]

$$\begin{bmatrix}\varepsilon_x\\ \varepsilon_y\\ \gamma_{xy}\end{bmatrix} = [T]^T[S][T]\begin{bmatrix}\sigma_x\\ \sigma_y\\ \tau_{xy}\end{bmatrix} = [S']\begin{bmatrix}\sigma_x\\ \sigma_y\\ \tau_{xy}\end{bmatrix} \quad (3)$$

$$T = \begin{bmatrix}\cos^2\theta & \sin^2\theta & 2\sin\theta\cos\theta\\ \sin^2\theta & \cos^2\theta & -2\sin\theta\cos\theta\\ -\sin\theta\cos\theta & \sin\theta\cos\theta & \cos^2\theta-\sin^2\theta\end{bmatrix} \quad (4)$$

$$S = \begin{bmatrix}S_{11} & S_{12} & 0\\ S_{12} & S_{22} & 0\\ 0 & 0 & S_{66}\end{bmatrix} \quad (5)$$

Where:

$\theta = \frac{\pi}{18} \approx 0{,}17453$ rad

The compliance matrix [S] is determined from the copper's material properties and transformed with $[T]^T$ and [T] to $[S']$ and furthermore transformed to the essential material properties in the bundle's coordinate system, i.e. (') for (S), (E), (G) and (v).

$$S_{11}=\frac{1}{E_x} \;,\; S_{22}=\frac{1}{E_y}=\frac{1}{E_z} \;,\; S_{66}=\frac{1}{G_{xy}}=\frac{1}{G_{xz}} \;,\; S_{12}=-\frac{v_{xy}}{E_x} \quad (6)$$

$$S'_{11} = S_{11}\cos^4\theta + (2S_{12}+S_{66})\sin^2\theta\cos^2\theta + S_{22}\sin^4\theta \quad (7)$$

$$S'_{12} = S_{12}(\sin^4\theta + \cos^4\theta) + (S_{11}+S_{22}-S_{66})\sin^2\theta\cos^2\theta \quad (8)$$

$$S'_{22} = S_{11}\sin^4\theta + (2S_{12}+S_{66})\sin^2\theta\cos^2\theta + S_{22}\cos^4\theta \quad (9)$$

$$S'_{66} = 2(2S_{11}+2S_{22}-4S_{12}-S_{66})\sin^2\theta\cos^2\theta + S_{66}(\sin^4\theta + \cos^4\theta) \quad (10)$$

$$E'_x = \frac{1}{S'_{11}} \;,\; E'_y = E'_z = \frac{1}{S'_{22}} \quad (11)$$

$$G'_{xy} = G'_{xz} = \frac{1}{S'_{66}} \quad (12)$$

$$v'_{xy} = v'_{xz} = E'_x \cdot S'_{12} \;,\; v'_{yz} = \frac{E'_y}{2\cdot G'_{yz}} - 1 \quad (13)$$

With all formulas and python calculations, the effective properties for copper and Kevlar are as follows in the table below. Kevlar is calculated with only the volume factor, while copper was calculated with the volume factor and helical winding. The materials copper and Kevlar behave mostly isotropic and not completely orthotropic.

Table 6: Resulting anisotropic properties with python packing generated and helical winding equation part 1

	Copper (soft) 0,91445 volume packing		Kevlar 29 & 49 0,907 volume packing
	No Helical Winding	Helically Winded	
E_x (Elasticity GPa)	114,306	114,013	99,77
E_y	114,306	114,013	99,77
E_z	114,306	114,013	99,77
v_{xy} (Poisson's ratio)	0,345	0,346677	0,356695
v_{xz}	0,345	0,346677	0,356695
v_{yz}	0,345	0,385333	0,356695
G_{xy} (Shear modulus GPa)	41,15	41,303	1,04305
G_{xz}	41,15	41,303	1,04305
G_{yz}	41,15	41,15	1,04305

Table 7: Resulting almost isotropic properties with python packing generated and helical winding equation part 2

	Copper (hard) 0,91445 volume packing	
	No Helical Winding	Helically Winded
E_x (Elasticity GPa)	118,878	118,715
E_y	118,878	118,715
E_z	118,878	118,715
v_{xy} (Poisson's ratio)	0,345	0,345896
v_{xz}	0,345	0,345896
v_{yz}	0,345	0,366549
G_{xy} (Shear modulus GPa)	43,436	43,523
G_{xz}	43,436	43,523
G_{yz}	43,436	43,436

2.4.4 Area moment of inertia

The area moment of inertia is a crucial variable for determining the bending stiffness on an object. This variable is based on the geometry and orientation, regarding its center, of the object when it is loaded. For a single fiber and the bundle, which is circular, the formula is $I = \frac{d^4\pi}{64}$ [22]. This would change dramatically if multiple materials were combined to receive a common value. The transfer formula $I_{tot} = \sum_{i=1}^{n} (I_{c,i} + A_i d_i^2)$ [22] is a good way to put a common moment of inertia over multiple objects. (A) is the area of each object, (d) is the distance from the fiber's centroid to the reference axis. (I_c) is the moment of inertia of each individual object, (n) is the total number of fibers and (i) is the currently targeted individual fiber. However, this formula is better applied if the objects are bonded to each other, which will make the object stiff. This implies that the objects cannot slip between, which can occur when there are loose fibers in a copper conductor. An I-beam is an example of combining rectangles in regard to the center with the transfer formula. Another formula could be used to determine the common moment of inertia that would be in a complete frictionless state. Using the $I_{tot} = n \cdot I_c$, which is the sum of all moments of inertia from every individual fiber in the conductor. This can give a very low value, which could be too flexible for the fiber component. The table below displays the different values of moment of inertia with the default value of the bundle diameter, value after the transfer formula, value after the sum of all individual fibers and a downscaled value of the transfer formula value. The downscaled value will be used for the desired FEA simulation in order to reach a particular displacement. The values of fiber diameter, bundle diameter and number of fibers are available in the same Python script that generated the volume package factor, Appendix C.

Table 8: Area moment of inertia for Copper and Kevlar

Formula	$I = \frac{d^4\pi}{64}$	$I_{tot} = \sum_{i=1}^{n} (I_{c,i} + A_i d_i^2)$	$I_{tot} = n \cdot I_c$	$I_{tot} = 0{,}007 \cdot \sum_{i=1}^{n} (I_{c,i} + A_i d_i^2)$
Copper (mm^4)	367,2	338,58	0,37	2,37
Kevlar (mm^4)	82,35	74,68	0,00033	0,52

2.5 Friction coefficients

For the FEM analysis, contacts will be required. Some simulations will utilize frictional behavior, meaning that the contacts require specific friction coefficients between the materials. The static friction coefficients will be targeted for the simulations. The table below displays a wide range of friction coefficients for the materials that are used for this cable. The friction coefficients are determined from the references [9-12, 23-26] in Table 9 and furthermore assumed to singular coefficients in Table 10.

Table 9: Friction Coefficients for Selected Materials (Dry Conditions)

Material	**Counter Material**	**Friction Coefficient (μ_{static})**
Copper	Copper	1
Kevlar (29/49)	Polytetrafluoroethylene	0,2 - 0,4
TPU (Polyurethane)	Any plastic	0,4 - 1
PE (Polyethylene)	Metal or plastic	0,5 - 0,8

The TPU had a generally high friction according to the references [9-12], which made the decision to use the friction coefficient between Kevlar and TPU with 0,4 unreasonable. Polyethylene's friction is quite large, and the coefficient was mostly lower with metal compared to plastic, which was usually higher, hence the decision between copper and XLPE. XLPE with copper, the coefficient is lower compared to XLPE against itself. Not much research with Kevlar was available, therefore due to TPU's and XLPE's high friction, the coefficient was assumed greater than 0,4 in comparison to polytetrafluoroethylene. The table below is the decided friction coefficients between each material for the simulations. There was not much research on friction coefficients for Silica. Its friction coefficient with XLPE was therefore assumed to be 0,4.

Table 10: Used Friction Coefficients for Selected Materials (Dry Conditions) in FEA

Material	**Counter Material**	**Friction Coefficient (μ)**
Copper	XLPE	0,5
Kevlar (29/49)	XLPE	0,5
TPU (Polyurethane)	Kevlar (29/49)	0,7
XLPE	XLPE	0.6
XLPE	Silica (fused)	0,4
XLPE	TPU (Polyurethane)	0,3

2.6 Thermal - Previous Research and Methodological Validation

Previous research on submarine cable thermal behavior provides important support for the approach used in this thesis. Several recent studies underline the critical aspects of convection, electro-thermal modeling, and FEM simplifications. Together they form the foundation of the present analysis.

Ma et al. [2] developed a thermal circuit model for DC submarine cables with a specific focus on seawater heat transfer. Their work demonstrates that even small variations in the convective heat transfer coefficient (h) can produce substantial changes in the maximum conductor temperature. This finding supports the decision in this thesis to calculate using Rayleigh–Nusselt correlations instead of assuming a fixed value, ensuring that the cooling effect of seawater is modeled realistically. González-Cagigal et al. [3] validated an electro-thermal model compared to real measurements and achieved low error levels. Their approach, joule heating in the conductor, heat conduction through layers, and convection to seawater, match the structure used in this thesis. Following confirmation that the modeling chain is consistent with proven methods. Finally, Del-Pino-López et al. [4] carried out comprehensive 3D FEM simulations of submarine cables and explored how geometry and material detail affect computational performance and accuracy. They concluded that simplifications of geometry and material properties are not only acceptable but necessary to reach convergence and maintain feasible calculation times. This conclusion directly supports the strategy adopted in the present study, where effective material parameters and a reduced computational domain were introduced.

In summary, these three studies collectively strengthen the credibility of this study. Ma et al. emphasize the importance of explicit convection treatment, González-Cagigal et al. demonstrate that the same electro-thermal modeling chain has been validated with real measurements, and Del-Pino-López et al. confirm that FEM simplifications are a standard and accepted practice.

2.7 Boundary Conditions and Loading Application

The simulations from the FEA software will give an understanding of motion and confirmation in methods of transforming bodies into their effective material properties. Ansys Workbench will be the main software for FEA utilization. The simulations shall make an accurate replication of the experiment hosted by Chalmers University and its collaborative hosts [7]. Particularly bending and tension on the conductors on different occasions, while torsion and fatigue simulations shall be further studied in the future. Some thermal and electric simulations will be considered important for combining thermal and static bending and tension simulations.

The model is nonlinear. For further stabilization of a solution, the model can have commands implemented. The necessary commands will eventually be investigated for simulation improvements. Substep results cannot be as linear due to nonlinearity iterations. This could be improved by manually increase the minimum Substep number which could make the total result more linear, however result in increased solving time. By geometry settings, brick integration can have influence. This study will investigate further in its different settings due to the reason that frictional or frictionless will be applied as contact settings. Lastly, the Newton-Raphson method, from the “Nonlinear controls” settings, will also be investigated for its different influences. Other settings with influence might be highlighted after all simulations.

2.7.1 Static Structural

Bending and tension will be the main mechanical considerations for this research. Both will be replicated as the experiment to compare and conclude the method of transforming. According to the experiments, both bending and tension have been tested with a 400 mm 1kV cable. The simulations will therefore have the same model, 400 mm in length. Both will furthermore be analyzed on the conductors on three different occasions to understand the settings needed for the boundary conditions and differences in solid and beam conductors. Different moments of inertia and combined load of tension and bending will furthermore be tested for better understanding of settings and constraints.

The fully 1kV cable model will not run fully coupled bending and tension load cases. The analysis will focus on single-load cases (bending and tension separately) to establish stable solutions and to compare deformation trends. Extending the verified setup to coupled cases could be the next step.

Stress was considered conceptually but not analyzed in detail. The simulations focused on deflection to replicate experimental bending and tension behavior. Stress evaluation, including yield and fatigue, is proposed for future work.

2.7.1.1 Contacts

Including contacts will make the solution nonlinear, which will increase the solving time. Solid elements usually generate contact conditions automatically. However, with a combination of different 3D-elements like solid and beam, it is more accurate to manually apply contact conditions. The conductors and Kevlar bodies are in this study referred to as fiber components in this study. The fiber components are modelled as line bodies, please see Figure 3, which will make them into beam elements. The rest, like the optic fiber, insulation and the outer shell are solid elements. For simulation fulfillment, the contacts between solid and beam elements will be tested between friction and frictionless. Friction can improve the model's status of constraints as the simulation would be unstable during over- and under-constrained conditions. Simulations will be tested with frictional behavior with the coefficients from section 2,5.

The formulation will be investigated with the penalty-based method under the "Augmented Lagrange". This approach would maintain numerical stability during complex, nonlinear deformation and allows for slight interpenetration and micro-sliding. It could help to converge force, displacement, and moment during the solver's equilibrium iterations by implementing contact stiffness between the surfaces. This could result in no penetration and great stability simulation. To apply contact between the vertices of line bodies to a surface, the “Beam” formulation would be a better option. This is crucial for boundary condition of tension simulation as there are supported plates included for the purpose of equal strain. By applying the radius and material of the fiber component together with the bonded option, the contact could result in no slipping between the cable and the supported plates, please see Figure 7. Its influence will furthermore be investigated after the simulations.

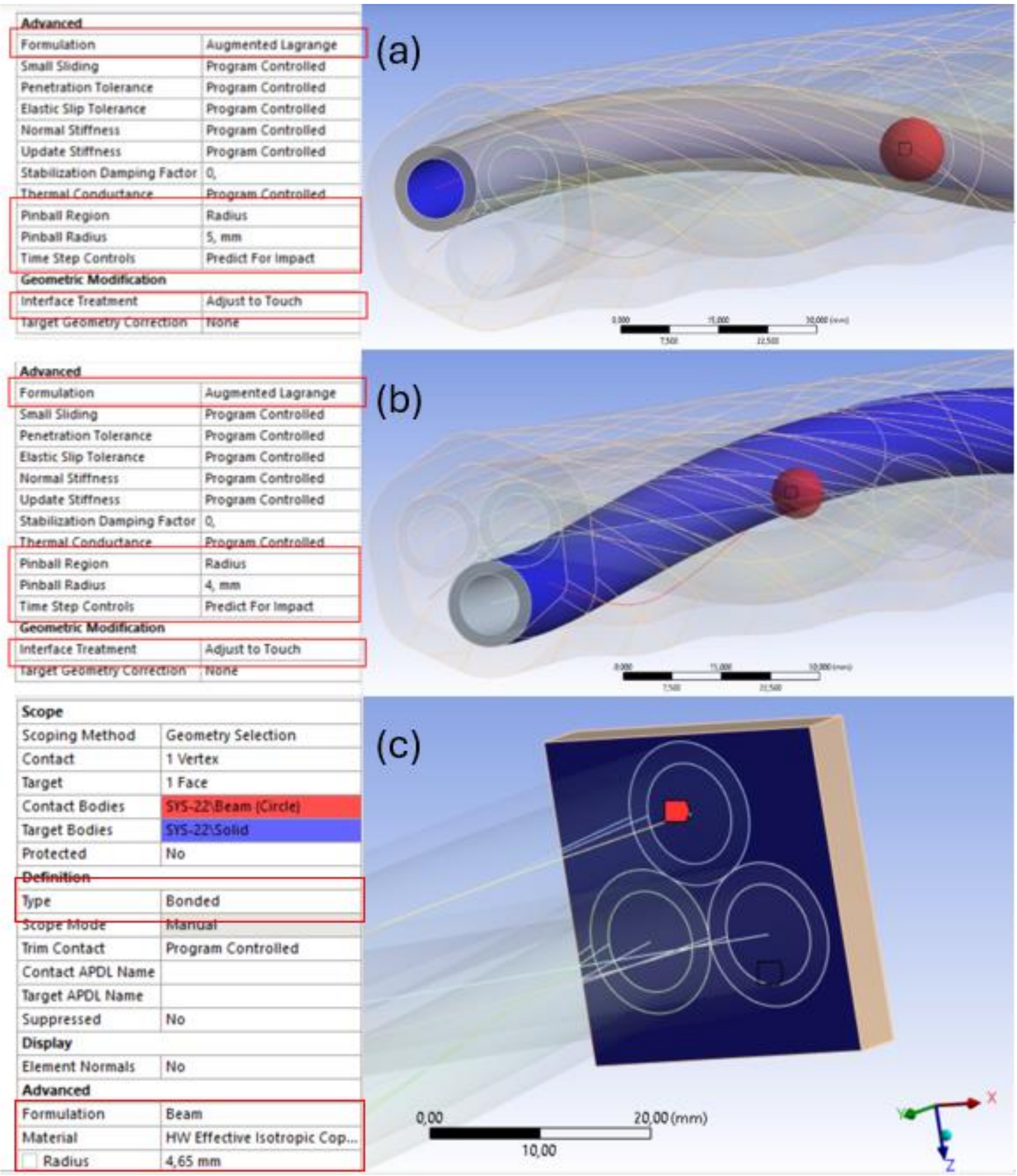

Figure 7: Contact settings and Pinball visualization

Furthermore, the pinball radius will be set manually larger than the conductor, however smaller than the insulation's outer radius. The pinball radius would help the solver to detect the target surface and perform its equilibrium iterations. The time step control is sometimes set to "Predict for impact" to perhaps detect the target surface easier and prevent large penetration. Lastly, the interface treatment is sometimes selected to "Adjust to touch" which would in practice support the contact to be closed. The more "closed" contact, the more stable the equilibrium iteration would be for the solver.

The simulations will utilize the "Contact tool", for the better understanding of applied contacts and how they could be verified for stability. The tool could aid how "closed" the contacts are before solving the model. The gap and penetration dimension should be zero or significantly small for a more stable solution. The less many gap and penetration, furthermore the smaller measure of gap and penetration, the more "closed" the contact is. Figure below illustrates an example of contact status in a 2D sketch from CAD software.

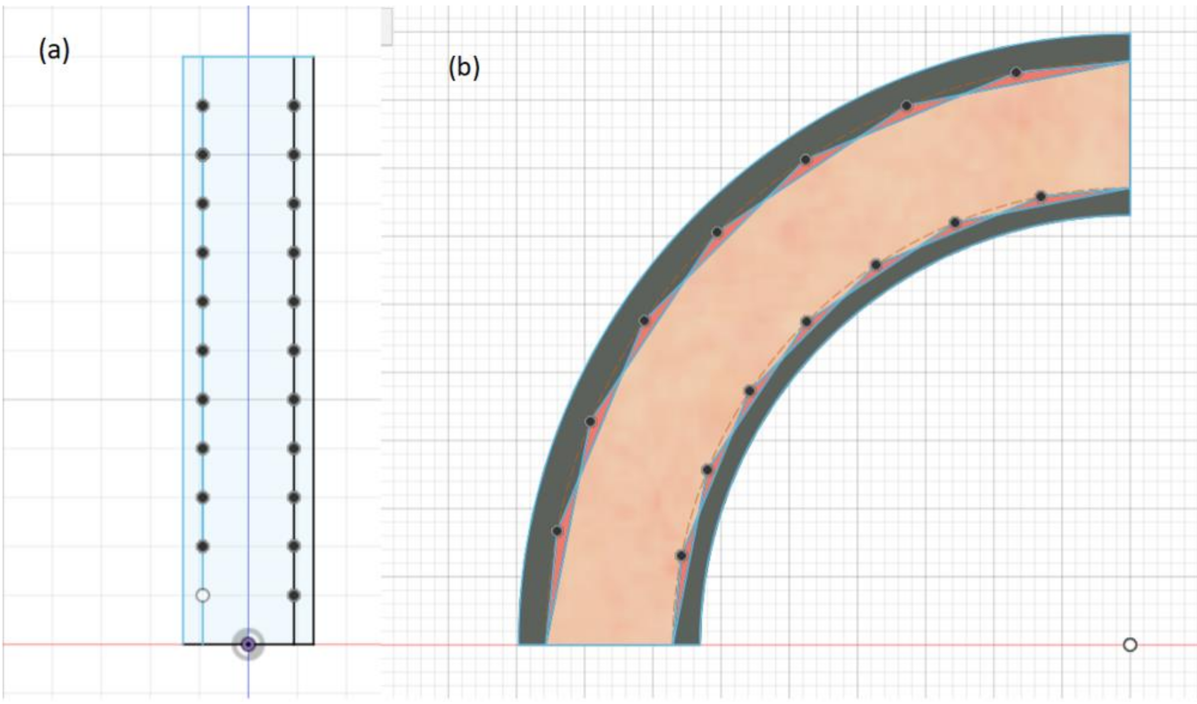

Figure 8: (a) More "closed" status, (b) Less "closed" status

Figure 8a is more "closed" due to its smaller gaps and penetration. Objects that are straight are more likely for less overlapping between elements compared to Figure 8b. Figure 8b is curved has larger probability for elements and nodes to overlap which causes gaps and penetrations. The red surface markings from Figure 8b are the gaps and penetrations. A finer mesh would make the measured gaps and penetration much smaller. However, it would cause a larger number of gaps and penetrations.

A combined analysis with steady-state thermal and static-structural has thermal conductivity included in the contact settings. This is needed for valid distribution of heat between bodies. 0 W/Km^2 would not distribute any heat from one 3D-body to another during a combination of steady-state thermal and a static structural simulation. If the contact is bonded, then the value is not accessible to edit. Frictional and frictionless status gives allowance to edit the thermal conductivity between the two applied surfaces or edges. The value was set from low to high value. Specifically, 10 to 1000000 W/Km^2.

2.7.1.2 Bending

The bending experiment used a roller on each side, 400 mm apart, and one roller pressing in the middle [7]. The model for the simulation will be 400 mm in length with marked vertices in the middle and on each side for symmetry. Due to the model being helically winded, there is no clear marking for force load and various boundary conditions. This could make the results unstable in motion and not look the same as the experiment. Rollers are furthermore not substantial due to increase in nonlinear solutions that could increase the solving time significantly. A force in the middle is furthermore not very good for the desired motion. A force on a surface or vertices in the middle will cause an edge pressure which will result in a less rounded bending.

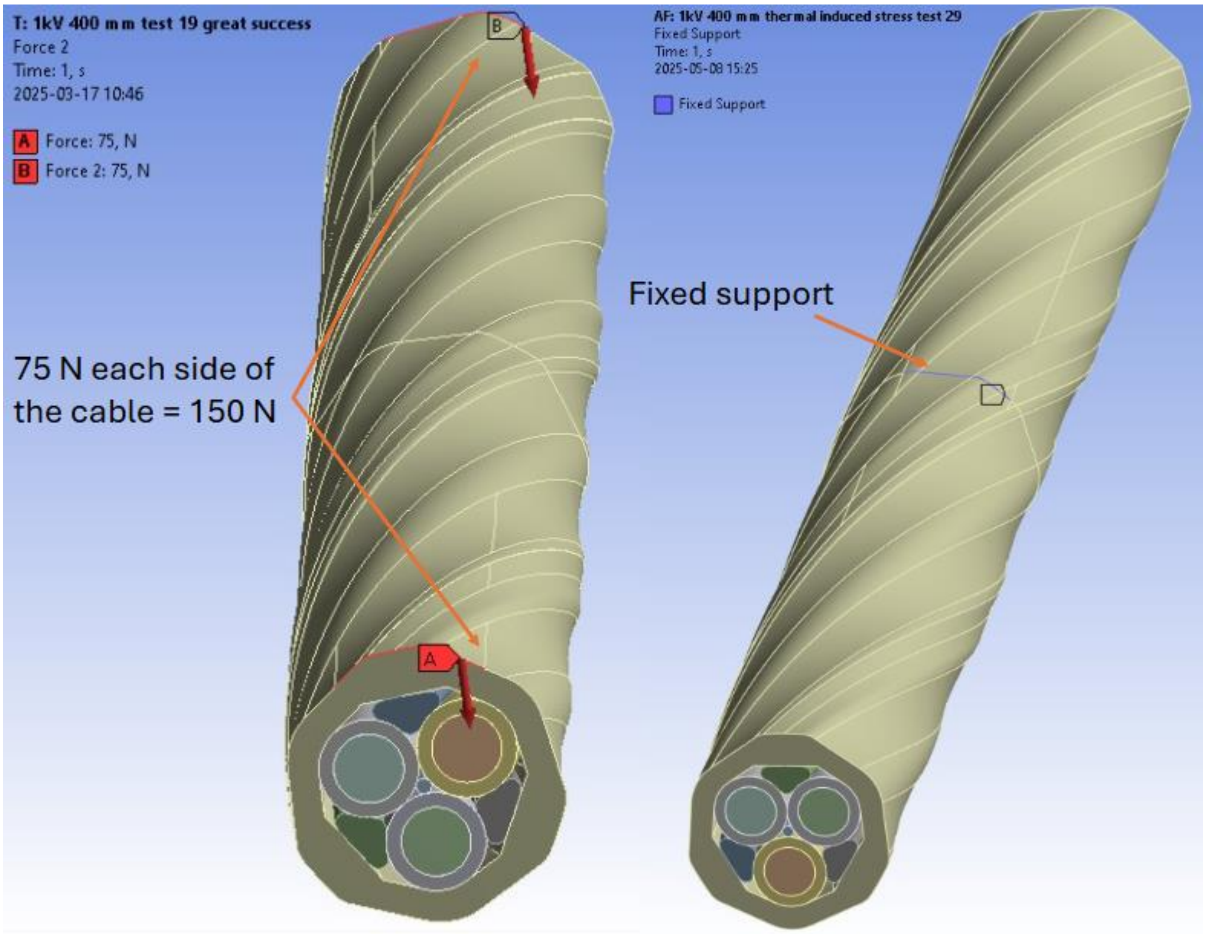

Figure 9: Fixed support and Force application for bending

Instead of a force in the middle, fixed support is placed. The force is divided in two and placed on each side. Target force is 150 N with 75 N on each side. Fixed support and force applications are placed on the TPU shell, see Figure 9. Displacement conditions have furthermore been placed on every other body in the middle, surrounding its circumference. The degree of freedom along the cable is locked. The transversal directions are free to move. Please see Appendix D for more details. Each body is sometimes set to "Full integration scheme" to investigate the influence by utilizing all nodes as integration points or with reduced number of integration points. Each contact is set with "Frictional" with the friction coefficients from Table 10. Mesh is set to quadratic and has an element size from 5 to 20 mm depending on the solving time. Reduced mesh is less computational heavy and is usually great for deformation analysis. Stress is more accurate with fine mesh but is more computationally heavy. In addition, the mesh defeature is sometimes set from 5 mm to default. Default value implies "program controlled", thus the software will set a suitable value. The span angle center is set to medium. This gives curvature-based refinement, meaning that cylinder objects get a finer mesh.

The bending for the conductors will use a force of 50 N on each side. This is to not exceed any stress limits and remain a stable solution on all occasions. In addition, the conductors will be simulated with solid and beam conductors separately which is the same as for straight fibers and helically winded fibers.

2.7.1.3 Tension

The experiment made by Chalmers University used different lengths. One of the lengths was 400 mm, where the ends were attached and pulled [7]. Similarly, the simulation will utilize a 400 mm in length cable model with additional support plates on each side. The support plates will provide equal directional strain in every component. The analysis and mesh settings are similar to bending simulations for a more linear and stable solving method. In addition, the contacts with support plates are "Bonded", thus every component can achieve equal strain. The inner side of one support plate has fixed support while the other plate has a load application of 17500 N along the cable direction. Please see Figure 10 for visualization. Additionally, there is a displacement condition on the same inner side of the support plate with the same load application. The transverse degrees of freedom on the displacement condition are locked. This makes sure that the cable does not twist during tension which could result in greater deformation, please see Appendix E for visualization.

The tension for the conductors will use a force of 10000 N on the plate side. Same as bending, it is to not exceed any stress limits and remain a stable solution on all occasions.

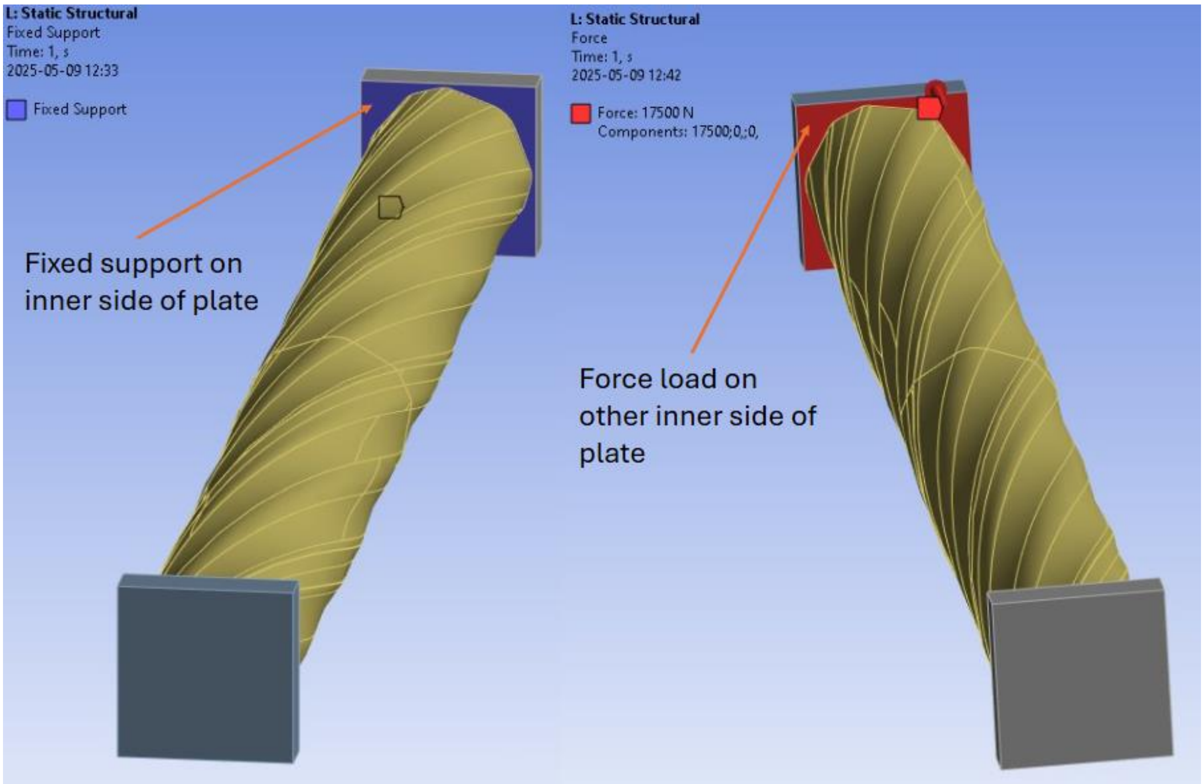

Figure 10: Fixed support and Force application for tension

2.7.2 Electrical-Thermal

The electrical-thermal analysis will be performed in ANSYS Workbench to replicate realistic operating conditions and evaluate how electrical loading influences the cable's thermal behavior. The process will consist of two main stages. Electrical analysis to calculate Joule heating and thermal analysis to model heat transfer through the cable structure.

To simplify the model, the copper conductor will be represented as a solid cylinder instead of multiple helically winded fibers. This setup would make the simulation faster and easier to manage while still providing accurate results for the cable's electrical and thermal behavior. This setup only lets electricity flow through the copper conductor, adds heat from Joule heating and moves that heat through the cable layers by conduction and convection. Air is not treated as a conductor, and these geometry and material shortcuts follow standard FEM practices [4].

The total electrical resistance of the conductor is calculated using $R = \frac{(\rho \cdot L_{twist})}{A_{tot}}$. The material resistivity, which is the total conductor length and is the cross-sectional area. Joule heating was then computed according to Joule's law $Q_{gen} = I^2 \cdot R$.

The electrical loading in ANSYS is implemented using a voltage-driven boundary condition with a potential of 1000 V applied to one end of the copper conductor, while the opposite end is assigned 0 V (Ground). Grounding is needed to have a reference potential and would ensure that the solver computes a unique current distribution through the conductor.

Joule heating is not automatically activated inside the electrical-thermal system. Instead, the electrical analysis in ANSYS would give a value of the internal heat generation value in the conductor. The value is calculated from the applied voltage and the conductor resistance. This value, expressed as a volumetric heat source, is manually applied in the thermal analysis. This approach would ensure that the thermal model used the exact same electrical losses that were obtained from the electric simulation.

Heat conduction was modeled through all cable layers, copper, XLPE, Kevlar, and TPU, using material properties from section 2,2. Each layer was built with the correct thickness so the model could show how heat moves from the conductor in the center out to the outer surface. In addition to conduction, cooling from the surrounding seawater is also included. This was done by adding convection on the outside of the TPU layer using a convection coefficient of h = 484,96 $W/m^2 \cdot K$, calculated analytically using Rayleigh-Nusselt correlations for natural convection in cold seawater. The surrounding temperature is set to 2°C [1], representing typical deep-water conditions where the temperature fairly stays constant. This is to simplify the study with a fixed temperature rather than a dynamic. Radiative heat transfer was neglected due to its negligible effect at operating temperatures (40 - 90 °C). These parameters ensure that the thermal environment accurately reflects realistic offshore operating conditions. Table 11 summarizes the key thermal boundary calculations used in the simulation. (Q_{gen}) is the heat generated. (I) is the electric current. (R) is the electrical resistance of the copper conductor. (ρ) is the electrical resistivity of copper from section 2,2. (L) is the length of the conductor and (A) is the cross-sectional area of the conductor.

Table 11: Thermal boundary preparations [1, 7, 8]

Step	Equation	Required inputs	Results
Joule heating	$R \cdot I^2$	I = 205 A R = 0,00010915	10,40 W/m
Electrical resistance	$R = \frac{\rho \cdot L_{twist}}{A_{tot}}$	$P = 1{,}68 \cdot 10^{-8}$ $A_{tot} = 0{,}00006789\ m^2$ $L_{twist} = 0{,}4002\ m$	0,00010915 Ω/m
A surface	$A_{sur}f = \pi \cdot d \cdot L$	d = 38 mm L = 400 mm	$0{,}04775\ m^2$
Convective heat transfer	$C_{conv} = h \cdot A_{sur}f \cdot (T_{cable} - T_{amb})$	$h = 484{,}96\ W/m^2{\cdot}K$ $A_{sur}f = 0{,}04775\ m^2$ $T_{cable} = 10°C$ $T_{amb} = 2°C$	185,25 W
Volumetric Joule heating (for FEM)	$Q_{vol} = J^2 \cdot \rho(T) = (I^2 \cdot \rho(T)) / A_{tot}^2$	I = 205 A $A_{tot} = 0{,}00006789\ m^2$	$4{,}5868\ W/m^3$

The main goal was to visualize how much the conductor and the outer surface heat up when current flows, and how the heat moves between the layers. The convective boundary was then used to evaluate how effectively the cable releases heat into the surrounding seawater. These results provide insight into the cable's thermal safety margins relative to material limits and help identify potential improvements in the insulation layout or the cooling capacity. This would be done by using Steady-State Thermal Analysis, an evaluated long-term thermal equilibrium under continuous electrical load to confirm safe operating temperatures by remaining below material limits. Furthermore, with the Transient Thermal Analysis, by capturing dynamic heating and cooling behavior during start-up and load variations, providing insight into thermal inertia and short-term fluctuations.

The implementation aimed furthermore to generate input data for combined thermal-mechanical simulations. This ensures that thermal effects are accurately represented when assessing mechanical performance under coupled loading scenarios.

2.7.2.1 Thermal-Electric

The steady-state thermal and electrical behavior of the marine cable is analyzed to see how heat is produced in the conductor and how it is released during operation. The focus was on the condition where the system reaches thermal equilibrium, meaning the heat created by the electrical current in the conductor is equal to the heat transferred to the surrounding seawater. This is important to make sure the cable stays within safe temperature limits and remains reliable over time. The cable model consists of a copper conductor surrounded by XLPE insulation, a Kevlar reinforcement layer, and an outer jacket made of thermoplastic polyurethane (TPU). The outer surface is in contact with seawater at a temperature of 2 °C [1]. The copper conductor carries an electric current that generates heat due to its electrical resistance.

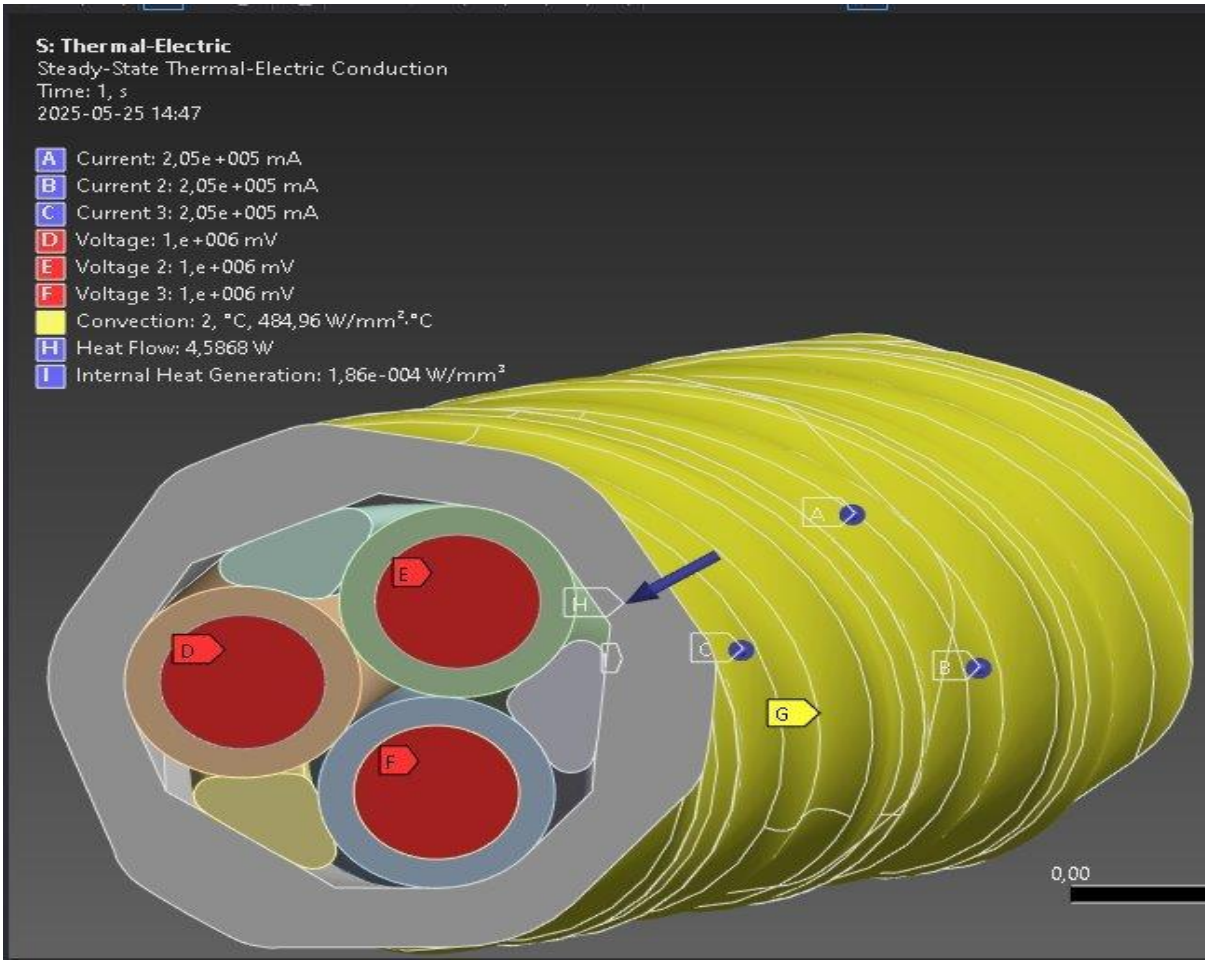

Figure 11: Thermal-electric boundary conditions

Heat is generated in the conductor due to Joule heating, which is defined from Table 11. In this case, it is assumed that a stable current over a 0,4 meter length of cable, and the heat generated in the conductor is then transferred radially outward through the XLPE, Kevlar, and

TPU layers before it is dissipated to the seawater. Heat is primarily dissipated through natural convection from the TPU surface to the surrounding seawater. The convective heat transfer rate is given by equation 14. (h) is the convective heat transfer coefficient, (A) is the surface area of the cable in contact with seawater and (ΔT) is the temperature difference between the cable surface and seawater.

$$Q_{conv} = h \cdot A \cdot \Delta T \tag{14}$$

To determine the heat transfer coefficient for natural convection, a step-by-step process involving several dimensionless numbers can be followed in Table 12.

Table 12: Step-by-step calculation process

Step	Formula	Calculation	Result
Step 1: Calculate Average Temperature	$T_{avg} = \frac{(T_{surface} + T_{seawater})}{2 + 273{,}15}$	$\frac{(10 + 2)}{2 + 273{,}15}$	279,15 K
Step 2: Thermal Expansion Coefficient	$\beta \approx \frac{1}{T_{avg}}$	$\frac{1}{279{,}15}$	0,003582 1/K
Step 3: Kinematic Viscosity	$\nu = \frac{\mu}{\rho}$	$\frac{1.673 \cdot 10^{-3}}{999{,}94}$	$1{,}67 \cdot 10^{-6}$ m²/s
Step 4: Prandtl Number	$Pr = \frac{c_p \cdot \mu}{k}$	$\frac{4218 \cdot 1{,}673 \cdot 10^{-3}}{0{,}561}$	12,58
Step 5: Grashof Number	$Gr = \frac{g \cdot \beta \cdot \Delta T \cdot D^3}{\nu^2}$	$\frac{9{,}81 \cdot 0{,}003582 \cdot 8 \cdot 0{,}038^3}{(1{,}67 \cdot 10^{-6})^2}$	$5{,}51 \cdot 10^6$
Step 6: Rayleigh Number	$Ra = Gr \cdot Pr$	$5.51 \cdot 10^6 \cdot 12{,}58$	$6{,}93 \cdot 10^7$
Step 7: Nusselt Number	$Nu = 0{,}36 \cdot Ra^{1/4}$	$0{,}36 \cdot (6{,}93 \cdot 10^7)^{1/4}$	32,85
Step 8: Convective Heat Transfer Coefficient	$h = \frac{Nu \cdot k}{D}$	$\frac{32{,}85 \cdot 0{,}561}{0{,}038}$	484,95 W/m²·°C
Step 9: Surface Area of Cable	$A = \pi \cdot D \cdot L$	$\pi \cdot 0{,}038 \cdot 0{,}4$	0,0478 m²
Step 10: Heat Transfer Rate	$Q_{conv} = h \cdot A \cdot \Delta T$	$484{,}95 \cdot 0{,}0478 \cdot 8$	185,26 W

This analysis was mainly carried out to verify that the cable does not overheat during continuous operation. By calculating how much heat is removed through convection, it was possible to determine whether the temperature remains below the insulation limit. The results also provided important input for the ANSYS simulations used to predict long-term thermal behavior, making this step an essential part of the design and validation process for marine power cables.

In the first stage, the thermal-electric model is used to apply the calculated heat input to the cable geometry and simulate how the heat spreads through the different layers. The same voltage and current values from the electrical model were used, and the total heat input was distributed evenly across the conductor region. Since the cable is surrounded by seawater, the ambient temperature in the simulation was set to 2 °C [1] to represent realistic underwater conditions. A convective boundary condition was applied to the outer surface to model cooling by the surrounding water. Heat transfer between the internal layers of the cable would also be included, based on the previously calculated values for material properties and geometry. This setup would ensure that the model realistically represents how heat moves through the cable structure in a submerged environment, providing a reliable basis for the steady-state thermal analysis.

2.7.2.2 Steady-State Thermal

The next stage in the simulation process was the steady-state thermal analysis, which used the heat input and boundary conditions from the thermal-electric model to calculate the temperature distribution once equilibrium was reached. This analysis assumes that the system has been operating long enough for the heat generated inside the conductor to be fully balanced by the heat dissipated to the surrounding seawater. The total heat flow through the model was calculated as 4,5868 W, which closely matched the output from the thermal-electric simulation. This consistency shows that the model would be thermally balanced and that the energy transfer between the simulation stages was accurately defined. A convective boundary condition with a heat transfer coefficient of 484,96 $W/m^2 \cdot K$ is applied to the TPU surface, representing strong cooling from the seawater.

2.7.2.3 Transient Thermal

The final step in the thermal analysis is a transient thermal simulation, which would give allowance to study how the cable heats up or cools down over time. Unlike the steady-state simulation, which assumes constant temperatures and thermal equilibrium, the transient model captures the system's dynamic thermal response, for example, how long it takes for the cable to reach its peak temperature after current is applied, or how quickly it cools when the load is removed.

In this simulation, the same heat generation from the copper conductor is used as in the previous steps, but instead of a fixed temperature result, the model calculated how the temperature changed across the cable layers at each step. This approach is particularly useful for understanding short-term events such as start-up, overloads, or power interruptions, where temperature can rise or fall quickly and potentially stress the materials. The boundary conditions remained consistent. Convective heat transfer to surrounding seawater and thermal conduction between the internal layers. Initial temperatures were set to match the ambient environment (2 °C), and the simulation was run over a defined time interval to observe how thermal energy builds up and spreads.

This transient thermal analysis is important because cables in real-world conditions do not always operate at a steady state. Load conditions can vary, and thermal inertia plays a significant role in how materials behave under changing temperatures. By running this simulation, it would gain insights into the thermal lag of the system, the speed of heat propagation, and the risk of thermal overshooting, all of which are critical for safe and reliable cable design.

2.7.3 Thermal-static

The result data from the steady-state thermal simulation can be fused together with a static-structural mechanical analysis. It will include internal stress and temperature combined as a new boundary condition to the overall simulation. The mechanical boundary conditions for bending and tension are the same as in sections 2,7,1,2 and 2,7,1,3 but with internal stress from temperature included. The materials have furthermore included thermal elasticity in the engineering data, and the contacts have the same, however different values of thermal conductivity. The simulations are to investigate the better method of combining the two boundary conditions for the probability of studying the mechanical behavior with thermal influence.

3 **Model Validation**

With much trial and error, the results were granted at utmost satisfaction. Some methods gave better results than other methods. This chapter delves into more details of what affected the results and its reliability.

3.1 Static structural

The results from with beam and solid elements were adherent to Chalmers' previous experiment with the cable. However, it was not completely identical. The moment of inertia is derived from Table 8. Table 13 derives with the downscaled value of the transfer formula from Table 8. Many simulations utilized an additional APDL command in the software, particularly the command NEQIT which sets the maximum number of equilibrium iterations.

Table 13: Most options used for the settings

Settings	**Used Option**
Moment of inertia	Copper: 2,37 mm^4 Kevlar: 0,52 mm^4
Contact formulation	Augmented Lagrange
Pinball radius (Often targeted)	Copper: 5 mm Kevlar: 3,6 mm
Time step control	Predict for impact
Interface treatment	Adjust to touch
Newton-Raphson nonlinear control	Unsymmetric stiffness matrix
Brick integration	Full
Substep control (Often targeted)	Minimum: 20 Maximum: 40
APDL Command	NEQIT, 200

Up to 50 simulations with many trials and errors were made to analyze bending and tension in the cable model. The table above is a list of the most used settings which, for instance, gave results in Figure 12 and Figure 13. The highlighted settings gave the most stable and realistic results by combining beam and solid elements. The settings were the most crucial for time consumption. Some combinations of settings could be up to 40-60 minutes while others were 10-20 minutes. The settings are further discussed in section 4,3.

Table 14: Exported Contact Tool result example

Name	Contact side	Type	Status	Number contacting	Penetration (mm)	Gap (mm)	Geometric Penetration (mm)	Geometric Gap (mm)	Resulting Pinball (mm)	Real constant
Component1\Body8 To Component1\Body11	Contact	Frictional	Closed	1	3.20E-04	0.00E+00	0	0.00E+00	1.2908	46
Component1\Body8 To Component1\Body11	Target	Frictional	Inactive	N/A	N/A	N/A	N/A	N/A	N/A	47
Component1\Body7 To Component1\Body11	Contact	Frictional	Closed	82	1.07E-02	0	1.07E-02	1.27E-05	4.027	44
Component1\Body7 To Component1\Body11	Target	Frictional	Inactive	N/A	N/A	N/A	N/A	N/A	N/A	45
Component1\Body6 To Component1\Body7	Target	Frictional	Closed	161	1.46E-02	0	1.46E-02	5.93E-05	5.1902	43
Component1\Body6 To Component1\Body7	Contact	Frictional	Inactive	N/A	N/A	N/A	N/A	N/A	N/A	42
Component1\Body5 To Component1\Body7	Target	Frictional	Closed	151	1.46E-02	0	1.46E-02	5.91E-05	5.3244	39
Component1\Body5 To Component1\Body7	Contact	Frictional	Inactive	N/A	N/A	N/A	N/A	N/A	N/A	38
Component1\Body5 To Component1\Body11	Contact	Frictional	Inactive	N/A	N/A	N/A	N/A	N/A	N/A	40
Component1\Body5 To Component1\Body11	Target	Frictional	Closed	247	5.87E-03	0.00E+00	5.87E-03	7.87E-06	2.1137	41
Component1\Body4 To Component1\Body7	Contact	Frictional	Inactive	N/A	N/A	N/A	N/A	N/A	N/A	34
Component1\Body4 To Component1\Body7	Target	Frictional	Closed	161	1.46E-02	0	1.46E-02	5.92E-05	5.3045	35
Component1\Body4 To Component1\Body11	Contact	Frictional	Inactive	N/A	N/A	N/A	N/A	N/A	N/A	36
Component1\Body4 To Component1\Body11	Target	Frictional	Closed	243	8.63E-03	0	8.63E-03	4.80E-05	2.1187	37
Component1\Body3 To Component1\Body8	Target	Frictional	Closed	1	2.24E-04	0	2.24E-04	7.50E-05	1.2908	31
Component1\Body3 To Component1\Body8	Contact	Frictional	Inactive	N/A	N/A	N/A	N/A	N/A	N/A	30
Component1\Body3 To Component1\Body7	Target	Frictional	Closed	84	1.04E-02	0	1.04E-02	7.91E-05	4.0168	29
Component1\Body3 To Component1\Body7	Contact	Frictional	Inactive	N/A	N/A	N/A	N/A	N/A	N/A	28
Component1\Body3 To Component1\Body6	Target	Frictional	Inactive	N/A	N/A	N/A	N/A	N/A	N/A	27
Component1\Body3 To Component1\Body6	Contact	Frictional	Closed	145	4.87E-03	0	4.87E-03	4.53E-05	1.5753	26
Component1\Body3 To Component1\Body5	Contact	Frictional	Closed	143	7.30E-03	0.00E+00	7.30E-03	2.41E-05	1.5804	24
Component1\Body3 To Component1\Body5	Target	Frictional	Inactive	N/A	N/A	N/A	N/A	N/A	N/A	25
Component1\Body3 To Component1\Body11	Contact	Frictional	Near Open	0	0	8.97E-04	0	8.97E-04	1.7576	32
Component1\Body3 To Component1\Body11	Target	Frictional	Inactive	N/A	N/A	N/A	N/A	N/A	N/A	33
Component1\Body2 To Component1\Body8	Contact	Frictional	Inactive	N/A	N/A	N/A	N/A	N/A	N/A	20
Component1\Body2 To Component1\Body8	Target	Frictional	Near Open	0	0.00E+00	1.18E-03	0.00E+00	1.18E-03	1.2908	21
Component1\Body2 To Component1\Body7	Target	Frictional	Closed	84	9.87E-03	0	9.87E-03	3.42E-05	4.035	19
Component1\Body2 To Component1\Body7	Contact	Frictional	Inactive	N/A	N/A	N/A	N/A	N/A	N/A	18
Component1\Body2 To Component1\Body6	Target	Frictional	Inactive	N/A	N/A	N/A	N/A	N/A	N/A	17
Component1\Body2 To Component1\Body6	Contact	Frictional	Closed	158	7.36E-03	0	7.36E-03	8.00E-06	1.7716	16
Component1\Body2 To Component1\Body4	Contact	Frictional	Closed	134	4.71E-03	0	4.71E-03	8.39E-06	1.7735	14
Component1\Body2 To Component1\Body4	Target	Frictional	Inactive	N/A	N/A	N/A	N/A	N/A	N/A	15
Component1\Body2 To Component1\Body3	Contact	Frictional	Near Open	0	0.00E+00	7.62E-03	0.00E+00	7.62E-03	1.53	12
Component1\Body2 To Component1\Body3	Target	Frictional	Inactive	N/A	N/A	N/A	N/A	N/A	N/A	13
Component1\Body2 To Component1\Body11	Contact	Frictional	Near Open	0	0.00E+00	2.52E-03	0	2.52E-03	1.7507	22
Component1\Body2 To Component1\Body11	Target	Frictional	Inactive	N/A	N/A	N/A	N/A	N/A	N/A	23
Component1\Beam (Circle) To Component1\Body3	Target	Frictional	Inactive	N/A	N/A	N/A	N/A	N/A	N/A	0
Component1\Beam (Circle) To Component1\Body3	Contact	Frictional	Closed	81	1.47E-15	0	0	4.5973	6	50
Component1\Beam (Circle) To Component1\Body2	Contact	Frictional	Closed	81	1.47E-15	0	0	4.5187	6	52
Component1\Beam (Circle) To Component1\Body2	Target	Frictional	Inactive	N/A	N/A	N/A	N/A	N/A	N/A	0
Component1\Beam (Circle) To Component1\Body11	Contact	Frictional	Closed	81	1.47E-15	0	0	4.5971	6	48
Component1\Beam (Circle) To Component1\Body11	Target	Frictional	Inactive	N/A	N/A	N/A	N/A	N/A	N/A	0

- White: No risk of instability
- Grey: Only considered for MPC or Normal Lagrange formulation
- Yellow: Small risk of instability
- Orange: Moderate risk of instability

The table above is directly exported from a contact tool status illustration before a simulation. It displays a summary of statuses for each applied contact to the model. The grey highlights are neglected unless “MPC” or “Normal Lagrange” formulation settings are utilized. Yellow and orange highlights indicate risks of convergence instability, but it is still acceptable to utilize. This illustration example gave a more stable solution with overall low time consumption. There are risks of instability but still acceptable with an average of 20 minutes’ solving time. The penetration and gap distances were the most usable indications to improve contact formulations. The column “Real Constant” acted as an internal identifier for the solver. Suspecting that the value of a “Real Constant” is an identifier for a set of settings and the resulting gap, penetration, geometric gap, geometric penetration from Table 14.

The target bending deformation was approximately 45 mm with a bending force of 75 N on each side. Both the cable model successfully reached the target, however the linear deformation under different loads separately does not coincide as well as the physical cable. This can depend on the effect of the moment of inertia in the fiber components if it is helically winded. Helically winded fibers would give the overall cross-sectional area along the fiber another shape. Therefore, another moment of inertia that is mainly stiffer depending on the fiber’s coordinate in the conductor.

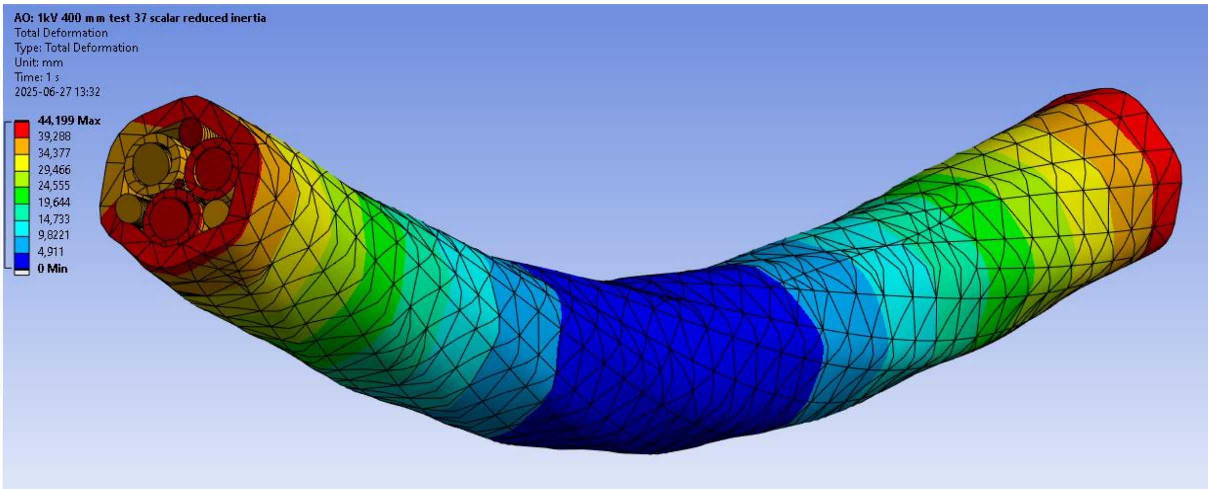

Figure 12: Bending results with Beam and Solid elements

Consequently, the tension did not receive a complete equal strain. Some slipping by the fiber components bonded to the support plate did slip a few microns away to the target deformation. Many simulations showed that the incorrect copper was implemented. Mainly the softer version of the C10100 pure copper was mostly utilized. The finalized results use the harder version of the C10100 which resulted in a more promising state. The beams with user-defined data, like reduced moments of inertia, did not report any stress and strain directly to the beam components after solution completion. Instead, the stress and strain data was sent to "Solution coordinate system" which could not be received afterwards. This was highlighted from a warning message after a simulation. Analyzing the solution information did not highlight any other additional information to receive the stress and strain data.

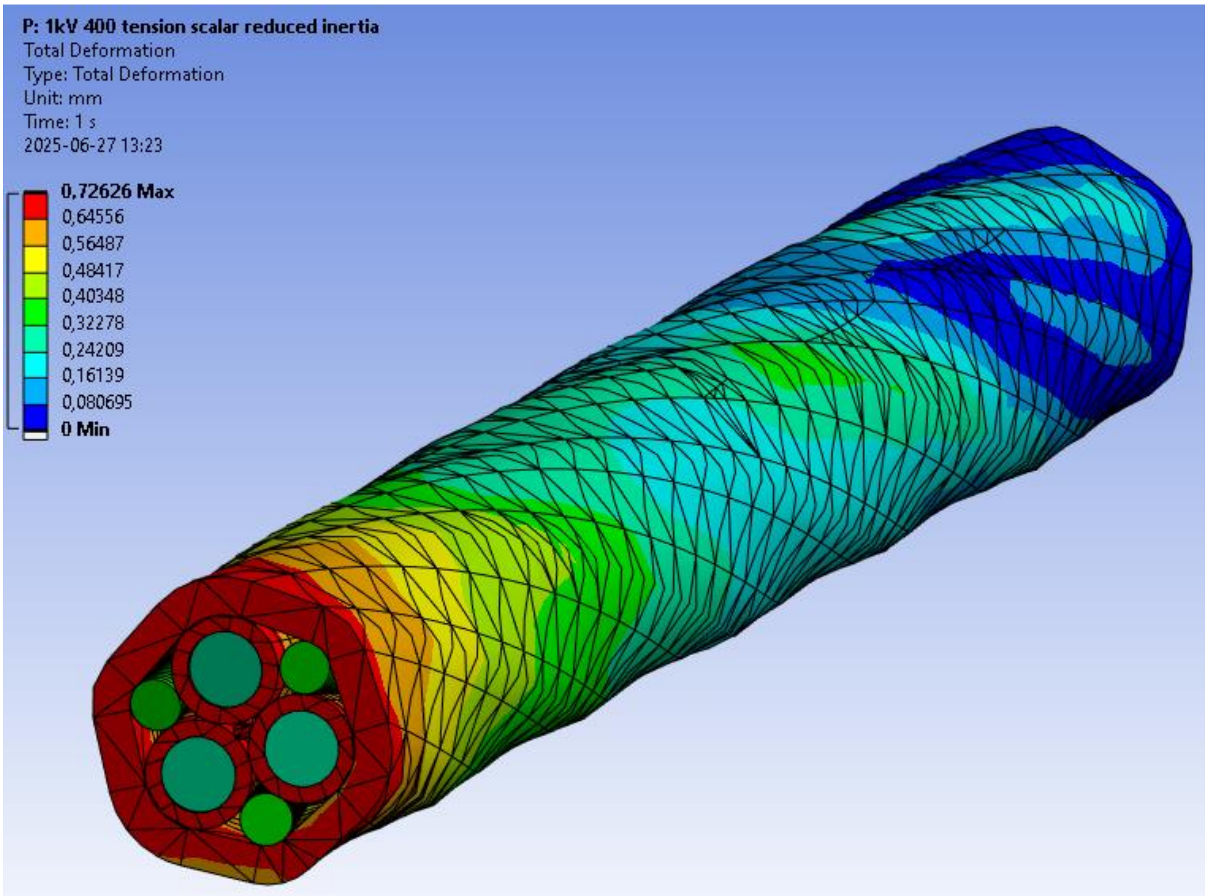

Figure 13: Tension results with Beam and Solid elements

This resulted in graphs comparing the experiment with the 3,6kV cable that was hosted by Chalmers. The dimensions between 1kV and 3,6kV are closely similar, which is why they were used for comparison. In comparison, the simulation results do not follow as much as anticipated. The Beam method is close to reference data but is still not considered a good foundation. Bending had some good comparisons but in relation to tension, the alignment is not promising.

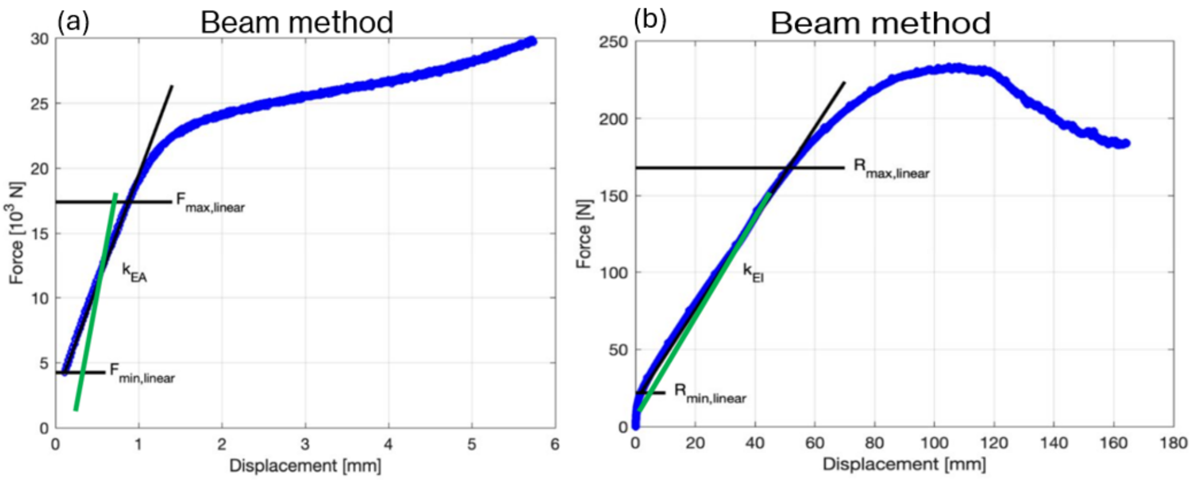

Figure 14: Data comparison with Chalmers experiment (blue) as background [7]. (a) Tension (b) Bending

The conductors gave a great understanding in motion and solving behavior. A total of 24 simulations were done with different fiber layouts, 3D-element and stress application. This was to mainly investigate the differences in result data of deformation, equivalent stress and solving time, please see the diagrams. C10100 is the material. HW is if the material is helically winded or not. B is for bending and T is for tension.

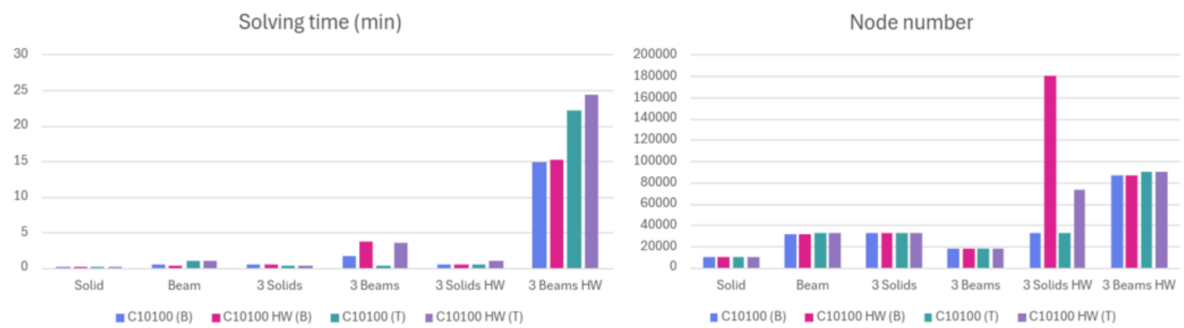

Figure 15: Solving time and Node number from each simulation

As expected, the solving time and node number is significantly lower for the singular conductor in comparison to the 3 conductors. The 3 Beams HW' C10100 HW (B) and C10100 HW (T) had some issues. This is probably from a poor 3D-file that affected the mesh negatively and therefore the solving time. Interestingly, the singular beam conductor had more nodes in its generated mesh in comparison to its solid counterpart. This obviously caused the solving time to increase for the beam model. However, the 3 Beams have lower nodes in comparison to 3 Solids. Yet the solving time is higher for the 3 Beams in comparison to the 3 Solids. This can be due to contacts that are not as closed in the 3 Beams. Consequently, the amount of nonlinear equilibrium iterations increases and thereby increases the solving time. The 3 conductor HW has, as anticipated, much more nodes for better curvature mesh alignment which consequently affects the contacts “closed” status poorly and thereby affects the solving time significantly.

In addition, there is data for deformation and equivalent stress for each simulation. Both show very similar results. Some minor micro differences have resulted in the counter 3D solid element. This can be due to the mesh quality between beam and solid elements. Beams have one-dimensional node distribution in its center axis while solid cores have nodes all over their 3D-body. Resulting in a more distributed placement, and usually in an increased number of nodes. Differences in HW are not as expected for bending. Helically winded fibers are typically providing a stiffer bending however a weaker tension. This can be shown in the tension simulations. This implies that helically winded coppers should have a larger moment of inertia in order to behave stiffer. The tension simulations showed more slipping between the conductors and the supported plate. During these simulations the “Beam” formulation was more used and resulted in much less sipping.

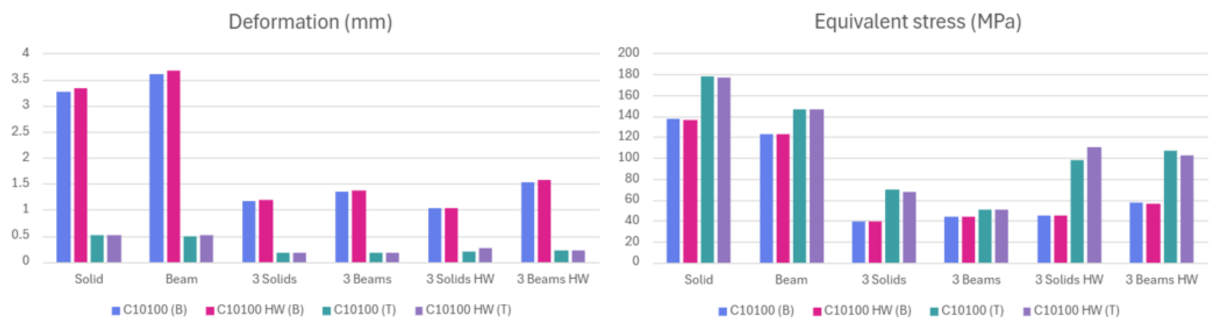

Figure 16: Deformation and Equivalent stress from each simulation

The singular beam and 3 beams HW models were targeted for different moments of inertia in its cross-section. They include the default value that is based on geometry, the resulting inertia using the transfer formula in a bonded state, the sum of all fibers in a frictionless state and the minimum value that is allowed in the software. The number of nodes is all the same and the equivalent stress was neglected due to the focus being the change in deformation. In summary, a total of additional 16 simulations were made. The most change occurs by 68 mm^4 and lower. The simulations become somewhat more unstable by 68 mm^4 due to large penetration in the XLPE insulation, especially tension for 3 beams HW. This can be due to lack of constraints from the applied boundary conditions, which heavily affected the distributed results of solving time.

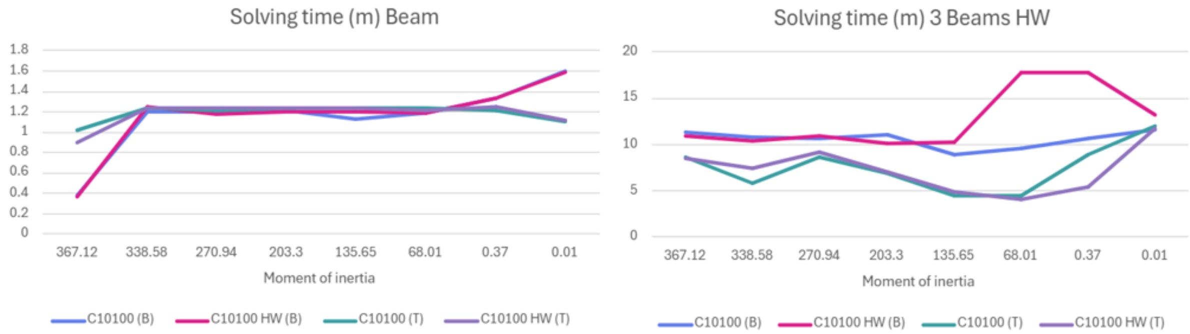

Figure 17: Solving time during lower moments of inertia

The deformation between both models has similar behavior in change under different moments of inertia. Same as the solving time, the most change occurs by 68 mm^4, meaning the closer to a frictionless state between the fibers the more flexible and similar it is to the expected bending behavior for cables. The difference in helical winding is so low that it can be interpreted as neglected.

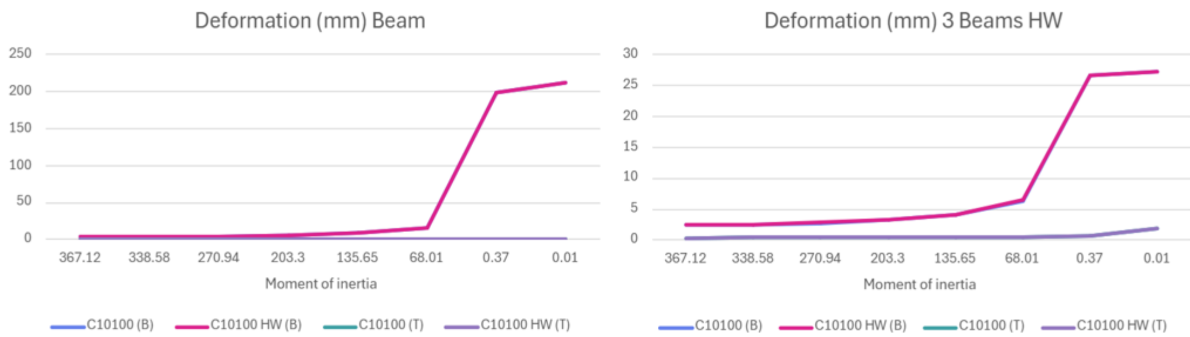

Figure 18: Deformation during lower moments of inertia

Three additional simulations proceeded with combined load of tension and bending. Unfortunately, they never reached a solution. The single conductor and 3 straight conductors could not converge the force to its criteria force even if the number of equilibrium iterations was increased to a much higher value. The total number of equilibrium iterations was increased to 400 and, according to Figure 19, the residual force stopped decreasing to reach the criteria force. The 3 helically winded conductors managed to reach force convergence during multiple substeps. This implies that simulation could reach a solution. However, the simulation was proceeded with another computer that did not utilize all processor cores which increased time consumption heavily. The simulation was stopped after 2 hours. Figure 19 shows bisections which redoes the calculations for the current substep.

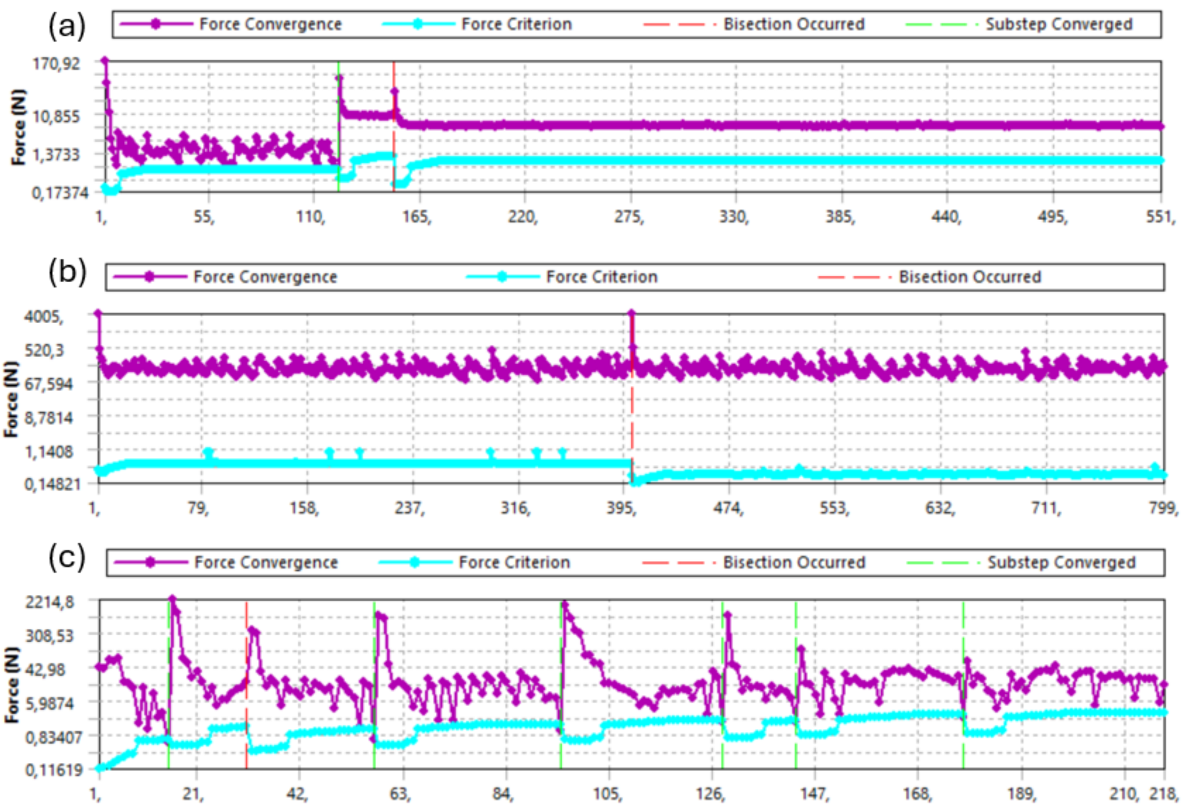

Figure 19: Force convergence process, (a) Single conductor, (b) 3 straight conductors, (c) 3 HW conductors

3.2 Thermal-Electric

The simulation used the boundary conditions and material parameters as defined in section 2,7,2,1. In this thermal-electric analysis, the electrical setup was applied to model how the heat generated within the conductor influences the cable's overall thermal behavior. The resulting Joule heating was transferred into the thermal model as a uniform internal heat source.

The Joule heat generation was calculated to be 4,7718·10^{-5} W/mm³, representing the amount of heat produced per unit volume inside the copper conductor. This internal heating was complemented by a heat flux of 0,0030629 W/mm³, describing how the heat began to move outward through the surrounding layers.

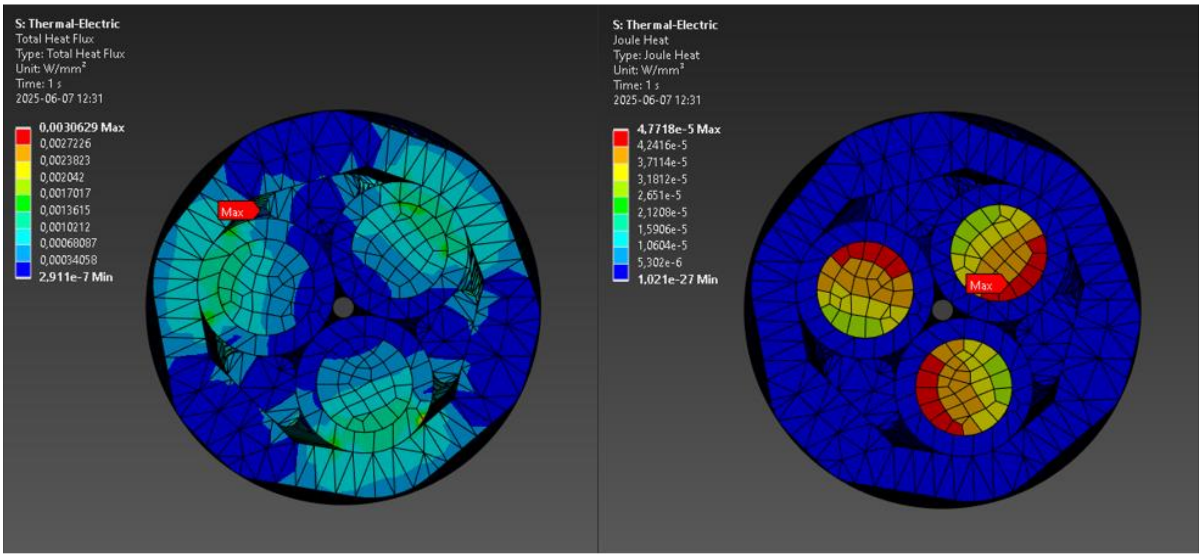

Figure 20: Thermal-Electric results

Overall, the simulation recorded a total heat flow of 4,5868 W through the system, based on the cable's material properties and geometry. As the heat moved outward, it passed through the XLPE insulation, the Kevlar reinforcement, and the TPU outer jacket, forming a clear radial temperature gradient. An important part of the thermal analysis was the convection between the seawater and the outer XLPE surface, which acted as the main cooling mechanism. Under these conditions, the maximum temperature at the surface of the conductor reached 37,161 °C, which is well within the safe operating range of the materials used, especially XLPE, which can be used continuously up to about 90 °C.

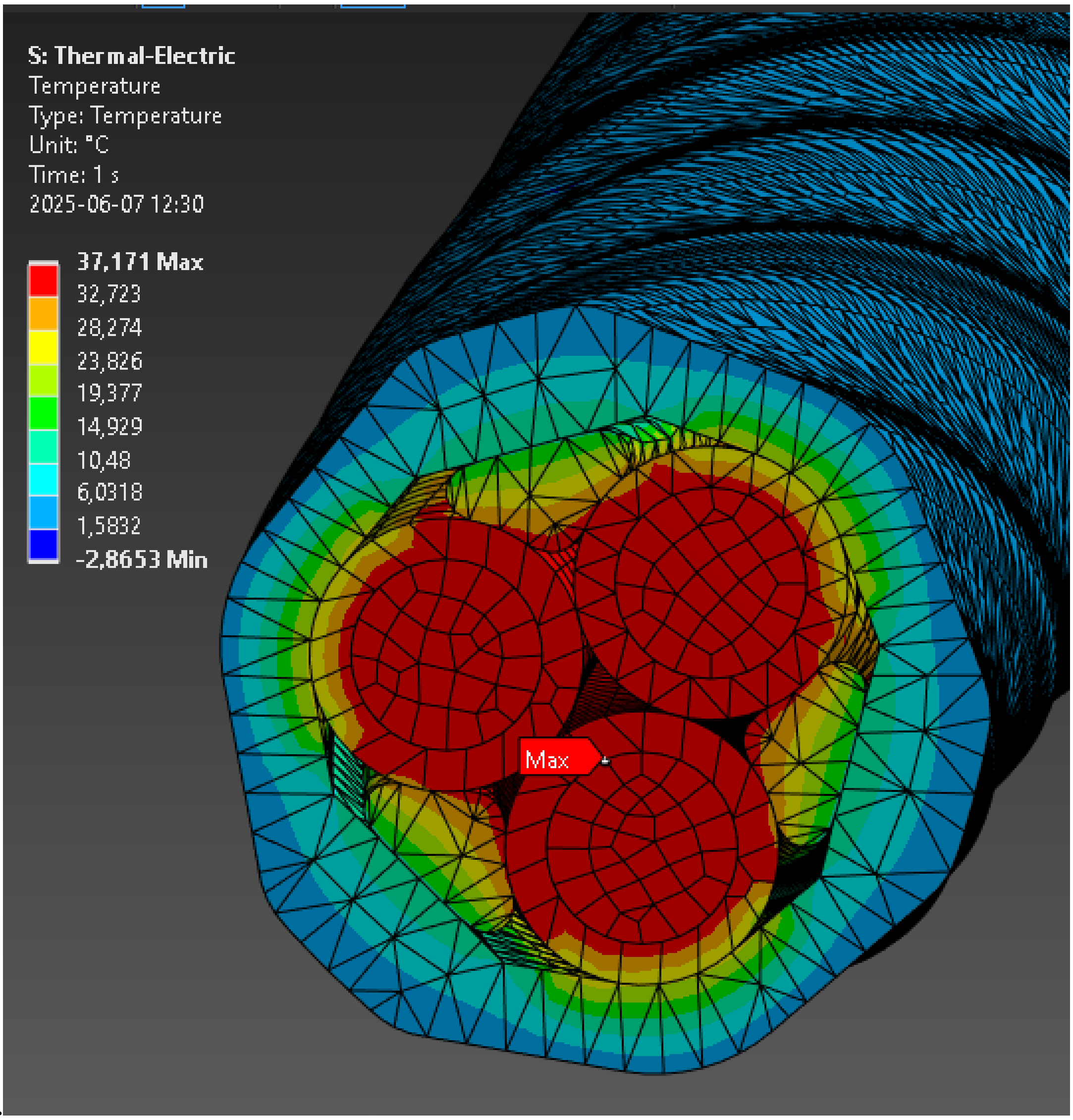

Figure 21: Thermal-Electric temperature

These results confirmed that both the electrical loading conditions and the thermal model were correctly defined. The heat was accurately generated, transferred through the cable layers, and released to the surrounding water by convection. This shows that the cable can handle the applied electrical load without exceeding its thermal limits and that the model is well prepared for further steady-state thermal analysis.

3.3 Steady-State Thermal

When the thermal-electric simulation was completed, the next step was to carry out a steady-state thermal analysis. This step evaluated how the cable behaves under continuous electrical loading after the system reached its thermal equilibrium, i.e. when the heat generated within the conductor is balanced by the heat dissipated to the surrounding seawater. The internal heat generation value of $4{,}7718 \cdot 10^{-5}$ W/mm^2, calculated from the previous step using a voltage of 1000 V and a current of 205 A, was applied as a constant thermal source.

As heat moved outward from the conductor (the copper) through the XLPE insulation, Kevlar reinforcement, and TPU outer jacket, the system gradually stabilized. The highest temperature in the model was recorded in the conductor, reaching 37,863 °C. This value is well below the maximum allowable operating temperature of 77 °C for XLPE and confirms that the cable design is safe from a thermal perspective and expected operating conditions.

The total heat flow through the system was 4,5868 W and closely matched the output from the thermal-electric simulation. This consistency indicated that the model was thermally balanced and validated the accuracy of the energy transfer between simulation stages. At the outer surface of the cable, cooling was provided through convection with surrounding seawater, which was modeled at an ambient temperature of 2 °C. We used a convection coefficient of 484,96 W/mm^2 to simulate the heat transfer from the cable's surface to the water, representing strong environmental cooling.

The steady-state thermal simulation confirmed that the cable can maintain thermal stability over time also under continuous electrical load. It also showed how effectively the surrounding seawater environment helps to remove heat from the cable surface and by that contributing to the cooling of the system. The realistic temperature gradient observed from the hot conductor core to the cooler outer layers helped visualize how heat travels through the different materials, reinforcing the importance of proper layer configuration and material selection. The close match between the steady-state thermal results and those from the earlier thermal-electric simulation proves the reliability of the model and the assumptions that were made. To summarize, this part of the study validated that the cable performs safely and efficiently in submerged conditions and that the simulation method is a reliable representation of performance in reality.

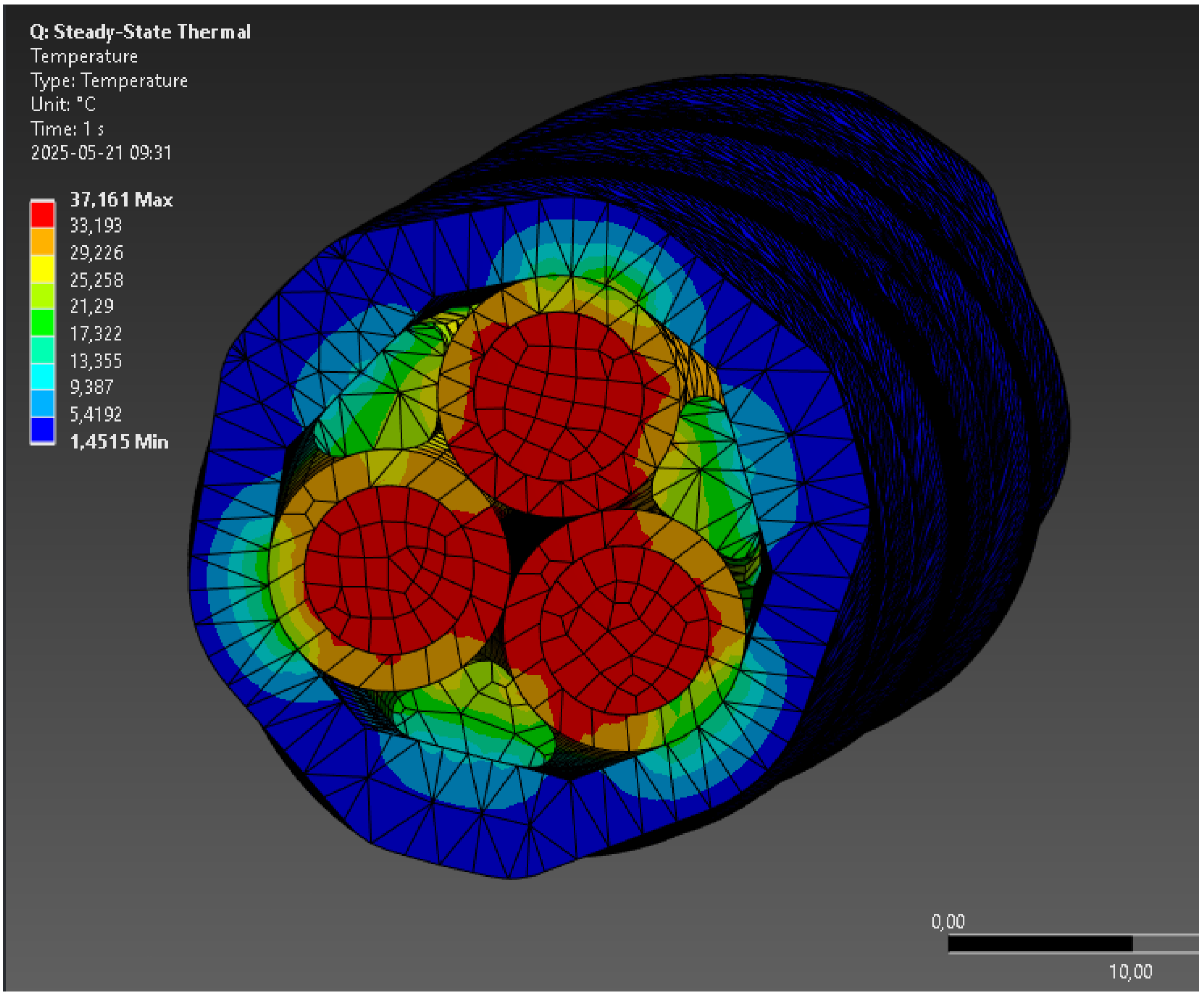

Figure 22: Steady-state Thermal results

3.4 Transient thermal

The transient thermal simulation used the same boundary conditions as the steady-state model to study how the temperature changes over time. After completing the steady-state analysis, this step examined how the cable responds when electrical power is first applied. While the steady-state model shows the final, stable temperature distribution, the transient simulation provides insight into how long it takes for the system to reach that condition and how the temperature evolves during the warm-up phase.

As time progressed, heat accumulated in the copper conductor and gradually transferred through the surrounding layers i.e. the XLPE insulation, Kevlar reinforcement, and TPU jacket. Due to the thermal resistance of these materials, the temperature increased steadily rather than suddenly. The conductor was the first to heat up, followed by a slower temperature rise in the outer layers, resulting in a smooth and realistic temperature gradient.

The simulation showed that the cable reached thermal equilibrium after approximately 58 minutes (3500 seconds). At this point, the maximum temperature in the conductor was 36,689 °C, which closely matched the steady-state value of 37,171 °C. This confirms that the model behaves consistently in both time-dependent and steady-state simulations and demonstrates that the cable can safely handle its thermal load without exceeding material temperature limits.

The results also showed that the cable heats up in a controlled and predictable way. No sudden temperature spikes or unstable behavior occurred during the start-up phase. Instead, the temperature gradually increased until equilibrium was reached, with the surrounding seawater providing effective and continuous cooling. These findings confirm that the cable remains thermally stable and reliable not only during steady operation but also when power is first applied or when the load changes.

3.5 Thermal-Static

The results for a combined thermal and static-structural analysis were both good and bad. The steady-state thermal needs the same components as in the static-structural simulation. The steady-state thermal was more successful if all components were solid elements and not combined with solid and beam elements. Beams only had distribution along its central axis, meaning that the heat distribution was not varied in the transverse directions of the cable. There was more distribution of heat with higher thermal conductivity in every contact. Some components were only minorly affected which did not abreast with the singular steady-state thermal analysis. The components were instead implemented with an average temperature from the steady-state thermal result data to receive a more realistic analysis with thermal application fused together with mechanical loads. Please see Appendix F for results.

4. **Discussion**

This chapter explains different viewpoints of the results and if there are topics of consideration that are crucial for change or just a general understanding of why the result data is affected in certain ways. Some are of deep importance depending on the aim of the topic while others are of acknowledgement.

One of the central goals of this project was to understand how the cable performs thermally under electrical load, and how that thermal behavior interacts with mechanical stress in a real marine environment. Through both steady-state and transient simulations, it was observed how heat is generated internally from electrical resistance, how it spreads through the different material layers, and how effectively it is dissipated into the surrounding seawater.

In the steady-state thermal simulation, the cable eventually stabilized at a temperature below the safe operating limit for all materials, confirming that the current design can handle continuous electrical load without overheating. In the transient simulation, it was possible to track how the cable warms up over time, reaching thermal equilibrium after approximately 58 minutes. This gradual increase in temperature gave valuable insight into how the cable behaves during startup and short-term electrical events, including conditions where thermal shock or rapid expansion could pose a risk to long-term reliability occur during sudden temperature changes in operation. Rapid heating from electrical load causes the copper conductor to expand faster than XLPE, Kevlar, and TPU layers, creating internal stresses. Repeated cycles can lead to insulation cracks, layer separation, and fatigue. The transient thermal analysis showed the cable takes nearly an hour to stabilize, making the initial heating phase critical. Mitigation includes gradual load ramp-up and selecting materials with closer thermal expansion properties.

What's particularly important is that thermal behavior directly influences the mechanical state of the cable via internal stress and thermal elasticity. As materials heat up, their mechanical properties change. For example, copper become slightly more resistive, and the mechanical stiffness of polymers like XLPE and TPU can decrease. This means that thermal and mechanical performance are closely linked, especially in offshore environments where cables experience constant motion, bending, and external forces in combination of thermal changes.

4.1 Thesis Improvements

Many FEA preparations could be improved for the desired result. The significance of data difference is not very high, however the methods to improve and state to improve are worth noting in order to reach finer accuracy or other essential data like stress and fatigue for future studies.

4.1.1 Model simplification

Many models have been generated and adapted. Along the journey, the models have been adapted and simplified for a less computational load.

An example is lines across the components. Mesh generation will utilize the lines as fixed reference points, which could increase the number of nodes in order to represent the geometry correctly. Many lines could be removed to reduce and make the simulation faster.

Shapes can determine the number of lines. For example, a rectangle utilizes four lines in its cross-section. But a circle utilizes only one. Aramid fiber components are examples of change in shape to circular in order to reduce lines which affected the mesh generation greatly.

4.1.2 Moment of inertia change and volume factor for helical winding

The cross-section area of an individual fiber changes if the fibers are layered in helical winding. The fact that the moment of inertia is based by the geometry, the area of helically winded fibers would be larger than the area of straight layered fibers. Image below shows an example of the cross-section between straight and helical winding in the second layer of five fibers. Helical winded fibers would look like an oval shape instead of complete circular shape. The eclipse has a larger area than a circle. This would affect the moment of inertia to be greater and therefore stiffer. This furthermore affects the used volume of the overall bundle area. In future studies, this is in great consideration to calculate the correct moment of inertia and volume factor for a fiber component.

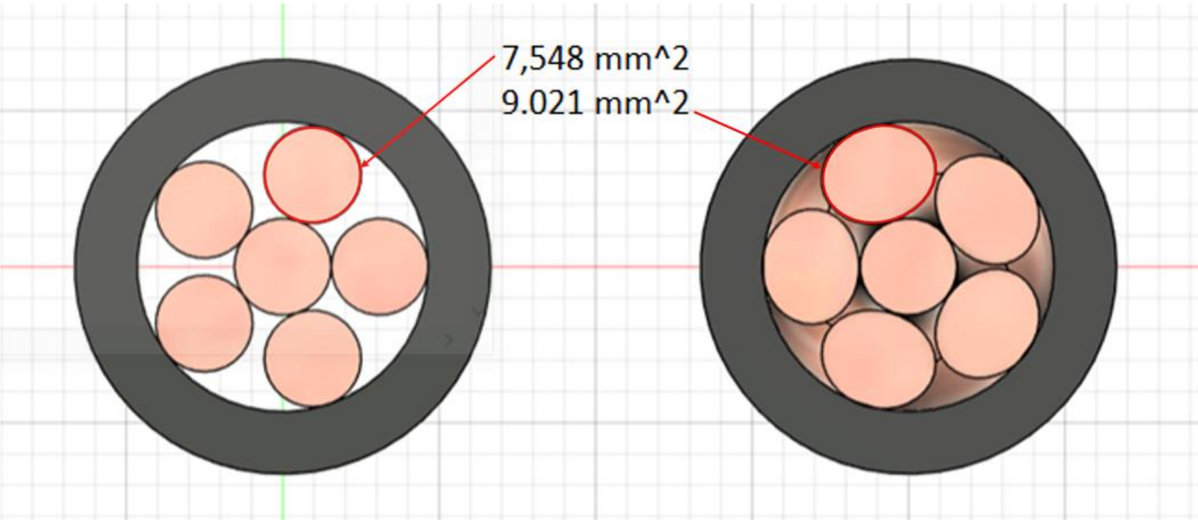

Figure 23: Cross-section visualization

4.1.4 Reducing Electrical Losses

One clear improvement for the cable design is to reduce the electrical losses that come from resistance in the conductor. The model used copper because it conducts well. But in reality, things like how the fibers are helically winded, the temperature increase, and small contact resistances can still cause power loss.

To address this, the conductor can be worked on to ensure that its geometry and material properties are optimized for minimal resistive heating. While a solid cylindrical model was used in simulations for simplicity, future improvements could include modeling the actual helically winded or fibered configuration more accurately. This would provide a better understanding of how the current flows between fibers and where additional losses might occur. This would be heavily time-consuming and is therefore recommended to model the materials' electrical and thermal properties effectively. Similar to the effective mechanical properties in the fiber components i.e. copper fibers and Kevlar.

Reducing these electrical losses is important not only for efficiency but also for controlling internal heat generation. Less resistive heating means lower temperatures in the conductor, which in turn reduces thermal stress on the insulation and extends the overall lifespan of the cable. This step helps to ensure that the cable performs reliably under electrical load, especially in long-term or high-current marine applications.

4.1.5 Thermal-Electrical Coupling

Another thing that could be improved is the dynamic change in the copper's electrical resistivity. When current passes through the copper, it produces heat, and that heat raises the temperature, which also changes the resistance of the copper material. Basically, the two effects influence each other.

In the current model, this coupling was included by using the heat generated from electrical input as a direct thermal source. However, the electrical resistivity of materials like copper can change with temperature. By refining the model to include temperature-dependent resistivity, the simulation would become more realistic, especially under high current or long-duration loading. This dependence can be expressed using a linear approximation $\rho(T) = \rho_0\left(1+\alpha(T-T_0)\right)$. Where ($\rho_0$) is the resistivity at the reference temperature (T_0) and (α) is the temperature coefficient of resistivity. Incorporating this relation allows the electrical and thermal behavior to be more accurately coupled within the model.

Improving this coupling helps ensure the simulation reflects how the cable behaves in operation. As temperatures rise, resistance increases, which causes more heat, a feedback loop is needed that can't be ignored in long-term performance analysis. Strong thermal-electrical coupling leads to more accurate predictions of temperature, power loss, and overall cable reliability.

4.1.6 Thermal Build-Up in High-Current Applications

In high-current applications a main challenge is how to handle thermal build-up, i.e. increasing temperature inside the cable. As current flows through the conductor the resistive heating increases, and if the heat does not dissipate efficiently the temperatures can rise quickly. Over time, this can stress the insulation materials and reduce performance of the cable and even shorten the cable's lifespan. In this project, it was found in the simulations that the internal temperature of the conductor increases steadily during load, especially during the early phase of operation. While the system eventually stabilizes thanks to convective cooling from the surrounding seawater, the initial phase is very important to understand. The initial phase shows how quickly heat accumulates and whether the materials can handle that stress before reaching equilibrium. To improve performance, the model can be refined to more closely examine how different loading, such as constant, pulsed, or fluctuating currents influences the heat build-up. This would make it possible to predict not just steady-state behavior, but also short-term thermal spikes that may occur during operational changes. Addressing thermal build-up is important for safe, long-term operation in subsea environments where cooling options are limited, and maintenance is difficult. Understanding and minimizing this risk ensures that the cable can handle demanding electrical loads without overheating or failure.

4.1.7 Thermal-static approach

The steady-state thermal analysis was modelled with most often solid elements and contacts with frictionless status. The higher value of thermal conductivity, with 1000,000 W/Km^2, distributed more heat between the components. However, some components were only minorly affected with 1000,000 W/Km^2. This means that thermal conductivity is perhaps infinite in bonded contacts.

The distribution of heat between solid and beam elements was lacking acknowledgement and understanding. The contacts between a solid and beam element include a gap from the central axis of the beam to the solid surface. The thermal conductivity between these elements is lacking and needs more research on how to make a combination of different elements more valid and accurate. Implementing the average temperature in all components was a reasonable approach to receiving realistic results.

4.2. Methodological Validation and Literature Comparison

The modeling approach used in this thesis is supported by previous research on submarine cable thermal behavior. The studies are a good reference to evaluating the choices made here and help explain that the results are according to previous results and findings.

Ma et al. [2] showed that even small changes in the convective heat transfer coefficient can have a big impact on conductor temperature. This supports the decision made not to assume a fixed value but instead calculate using Rayleigh–Nusselt correlations. This makes the cooling effect of seawater more realistic and that is critical for predicting safe temperature limits.

González-Cagigal et al. [3] validated an electro-thermal model against real measurements and achieved low error margins. Their approach, i.e. joule heating in the conductor, heat conduction through layers, and convection to seawater, is almost the same as the method used in this thesis. While this work did not include DTS validation, the similarity in methodology suggests that the results are consistent with proven approaches.

Del-Pino-López et al. [4] highlighted that simplifying geometry and material properties is necessary to keep FEM simulations stable and efficient. These simplifications allowed the simulations to run faster without losing the essential physics.

In short, the choices made in this work, i.e. explicit convection calculation, validated electro-thermal modeling principles, and controlled simplifications are in line with known practices. The results confirm that these decisions were appropriate for achieving accurate and computationally efficient simulations of marine cable behavior under realistic conditions.

4.3 Source of limits

The study involves some limitations that were not enlightened until the end of the study. Some limitations were noticed earlier on and were taken into consideration to not repeat mistakes in future studies.

The decision to model step by step was made to validate single-load behavior and numerics. This limits direct conclusions on combined loading and can be investigated in future work. Coupled load cases (bending + tension) were tried with the conductor models. It only resulted in increased time consumption and a higher probability of non-converged solutions.

Achieving convergence in nonlinear FEA does not guarantee physical correctness. While numerous trials and adjustments (mesh refinement, contact settings, substep control) were performed to obtain converged solutions for bending and tension, these results must be validated against experimental data to ensure physical accuracy. Convergence only indicates numerical stability, not that the model fully represents real-world behavior.

4.3.1 Twist sweep method approach

The twist sweep method is great to accomplish helical winding. However, it does not twist the cross-section of each fiber perpendicular with its individual central axis. The fibers' cross-sectional area instead follows the cable's central axis in parallel with the global cross-section plane. What was discussed in section 4,1,3 applies here. The conductors' cross-section shape should not be circular; it should have an oval shape. The purpose of accuracy could be increased by correctly modeling the components in helical winding.

4.3.2 Utilize the 3,6kV model

The graphs for the comparison results are based on the experimental results of the 3,6kV cable model that was hosted by Chalmers University. The original graphs are available from reference [7] and displays results only for the 3,6kV and not the other 1kV and 24kV cable that was also used for their experiment. Unfortunately, the results for specifically the 1kV cable are inaccessible through collaborative hosts with Chalmers. The reference [8] displays furthermore dimensions for the 1kV cable that was needed in order to model the cable in Fusion 360 and Ansys SpaceClaim. The difference between each measurement from the 3,6kV and 1kV were either equal or very small. This made it convenient to continue and acknowledge that the small differences in the results comparison data could be due to small measurement errors. If the inaccessible data from the collaborative hosts with Chalmers could have been reachable, the result data could have been further accurate.

4.3.3 Friction

One aspect from a mechanical perspective which was decided to be mostly excluded from the project scope to limit complexity, was how to handle friction in the simulation. Although it might seem like a small detail, the friction coefficient has an impact on how internal components of the cable interact under load. In a real cable, the copper wires, XLPE layer, Kevlar layers, and TPU jacket are all in contact with each other, and they don't just slide freely, there is resistance to motion. The static coefficient of friction for copper-on-copper contact under dry conditions is μ ≈ 1,0. Kevlar and TPU would be modeled with slightly higher friction, since both materials have rougher surfaces and tend to grip more.

Additionally, friction could give a much clearer picture of how loads are shared between wires and how the whole structure deforms under combined loading. Friction between all fibers could in theory affect the moment of inertia to act stiffer and generate internal stress if or when studying cables' strength and fatigue are desired.

Modeling friction properly would give an understanding on how much internal movement is happening inside the cable during mechanical stress and could help to evaluate if the design is effective in realistic conditions. This understanding is important for marine cables, which are constantly under dynamic loads from the ocean.

4.4 Analysis settings

The settings for analyzing a 3D-object under stress are crucial in order to reach an accurate solution. The setting of importance is mainly for static structural analysis to understand what methods, commands and values are valid for nonlinear solution models with behaviors like large deformation and sliding contacts.

4.4.1 Mesh

Mesh is the process to place nodes and elements distributed in a 3D-model so the solver can utilize the nodes and elements for its equations, based on the model's geometry and boundary conditions. Fundamentally, the more nodes and elements generated, the more computational heavier the solution will become. More equations are needed and the time consumption for a solution will be substantial. However, the finer mesh i.e. the more nodes and elements generated, the more accurate the solution will be. In this case with the cable model, the mesh has been something in the middle between coarse and fine status, in order to have sufficient results and not consume too much time. Coarse and fine mesh status are general terms used for finite element analysis. The element size for the cable has been between 1 mm to 10 mm, depending on the sizes of the components. The fiber components have been especially problematic in order to receive a sufficient "closed" contact status that is stable enough for the solver. The finer mesh will give a more "closed" contact status. However, the fact that the model is nonlinear, the solver will make a solution in "Out-core memory". This means that the solution will not be created with the support of the computer's random-access memory. The time consumption in comparison with "In-core memory" is significantly changed from 30 minutes to multiple days as an example. A coarser mesh is therefore more sufficient. It cannot be too coarse, however. A too coarse mesh will make mush less "closed" contact status. This will make the time consumption in comparison with a little finer mesh, doubled from 30 minutes to 1 hour as an example. It is important to define individual mesh sizing on each component of the model in order to have an effective and stable solution for future studies. This regards furthermore the power properties of the computer that will be used for solving a simulation. The more random-access memory available, the finer mesh is possible to keep the solution in "In-core memory" territory. Notably, if more processing cores are used, the faster the solution which was noted in the 3 helically winded conductors, from section 3,1, while combining tension and bending.

4.4.2 Frictionless contacts

Contacts are usually autogenerated between two surfaces. It is possible to tune the settings so it can autogenerate contact between surfaces and edges. In this case, the cable model utilized many contacts between surface and edge. Particularly the beam center axes to the surface from a corresponding layer component. An example is the beam copper conductor and XPLE insulation or the Kevlar component with either XLPE insulation or the TPU shell. Unfortunately, there was a big gap between the edges and surfaces in order for the beam to utilize its full transverse volume. It is meant that the outer edge from the circular beam is to be in contact with the corresponding surface. The Ansys software, however, utilizes this with the right settings. The formulation was mainly "Augmented Lagrange" which enforces the contact penetration between each surface or edges to be zero [27]. Contact stiffness is therefore not always the dominant factor to accomplish zero penetration, meaning that an extra term is used in order to augment the contact force calculation [28]. This gave realistic results because of the cable's high compact structure. "Beam formulation" was used to bond the beams with the supported plate for the tension analysis. This formulation only works for bonded type contacts in which the topology will be stitched together with the targeted surface or edges [28].

The pinball radius is a spherical region around each contact detection point which is usually automatically calculated but can be incorrect depending on the complexity of the geometry. Inside the spherical region is where the contact forces and node interactions are calculated. The contacts for the cables would often exceed the pinball radius which would affect the other components and heavily affect the convergence. The pinball radius was therefore needed to be set within each thickness of components in order to not make the solution too unstable. For example, the conductors' pinball radius needed to be within the XLPE insulations. [29]

Time step control is a valuable setting to detect drastic changes in contact behavior after each step. This allows the solver to perform bisections depending on chosen option. The "Predict for impact" option was sometimes utilized, not acknowledging the setting's influence. It was later known of its impact for the solver to perform necessary bisections, by reevaluating with a time increment but also the minimal time increment to detect changes in contact behaviors [30]. For future studies, it is usually recommended if impact is expected within the contact for a model.

The interface treatment settings allow the user's desire to offset between the surface or edges on the contact [31]. The cable's components touch each other, meaning that the tolerance should be close to zero. Allowing the contacts to not have a large gap or penetration in between. Some contacts were already penetrating or had visible gaps. The "Adjust to touch" was sometimes used. It was however not known that the interface treatment setting would accomplish the desired touching behavior and not allow the components to penetrate each other or have gaps [31]. This was, on later simulations, crucial for contacts between beam and solid elements to appropriately utilize the right surfaces. Confidently, a highly complex model with many layers and contacts is of need for the "Adjust to touch" setting.

4.4.3 Newton-Raphson & Brick integration

A nonlinear model will solve the solution by calculating multiple iterations of equilibrium in order to converge in its current Substep. These iterations include the residual output of natural forces like force, moment, displacement etc. Depending on the applied loads and boundary conditions, the solver will utilize the necessary forces of nature that is sufficient for the solution. In this case with bending and tension, the force, moment and displacement are necessary for the solution to be accurate. The iteration includes a criterion for each residual output. If all residual output is below its equivalent criterion, then the solution for the current Substep is converged. The Newton-Raphson method is a numerical algorithm that calculates the roots for the residual outputs [32]. This includes the stiffness matrix in the calculations. The default setting for matrix structure is symmetric which is a faster option for solving solutions. However, it will heavily affect the iterations during nonlinear solutions [33]. It is possible to change the stiffness matrix to an unsymmetric structure, which was sometimes recommended by the Ansys software. By acknowledge, that would affectedly support the iterations for stable convergence in nonlinear models, such as sliding contacts with friction or frictionless. This can however affect the computational load heavily in the random-access memory [34].

The options for brick integration scheme varies depending on what kind of 3D element that is implemented. SOLID186 is a homogeneous structural solid and is the usual 3D-element from CAD or CAM. It is the most suitable for irregular meshes and is usually generated in a brick structure [35]. With it comes the option to either utilize full integration or the default reduced integration. The reduced integration utilizes one Gauss integration point in each brick which is computationally faster, but the solution can cause an hourglass mode [36, 37]. Hourglass mode are distortions [38] that are unrealistic and can heavily affect applied nonlinear contacts with their "closed" status. Full integration utilizes all Gauss integration points which will cause more accurate behavior. However, the solution can display volumetric locking and can be more time-consuming for the solver. Full brick integration was sometimes used in this case, not knowing the solver would not affect the contacts negatively and not increase time consumption too heavily. Similar to the interface treatment with a high complex model with many layers and contacts, it is recommended to utilize full integration to not risk hourglass mode.

4.4.4 Local Coordinate settings

Most FEA software utilizes a global cartesian coordinate system that is applied to all components in the 3D-model. Local coordinate utilizes its own axis of direction in an applied component. It is mostly used for composite components with orthotropic material properties. The geometric orientation of the composite component can falsely interact with its material properties and the cartesian global coordinate system. Local coordinate system can in this case fix and properly establish a true interaction with the material properties and the cartesian coordinate system. However, a preview of the coordinate system along their helical winding was unsuccessful and therefore undetermined if the local coordinate system worked as expected. The fiber component's central axis is constantly changing in direction along the cable and made it unsure if the local coordinate systems axis was following the central axis in parallel all the way. More studies are needed for a better understanding of the local coordinate system's behavior in axis change along a component. A preview of the coordinate system is greatly supported to conclude a functional foundation of understanding with applied coordinate systems.

4.4.5 Other Nonlinear control settings

The default setting for step controls is program controlled, meaning that the solver will choose the amount of Substep that is necessary for a stable solution. Sometimes the solver could not manage the value of degrees of freedom in each node if the values are greater than a certain limit. This could be cleared with commands. However, the accuracy of the solution can be undetermined. Same is for the linearity of results through Substep. The values of degrees of freedom were possible to be lowered by increasing the amount of Substep manually. The solution would have increased time consumption. However, the probability of success is higher. Figure 24 visualizes the difference in linearity of results on the three helically winded conductors in function of time. One includes 22 Substep and the other includes 38 Substep. The solution with 22 Substep is not as linear as the solution with 38 Substep.

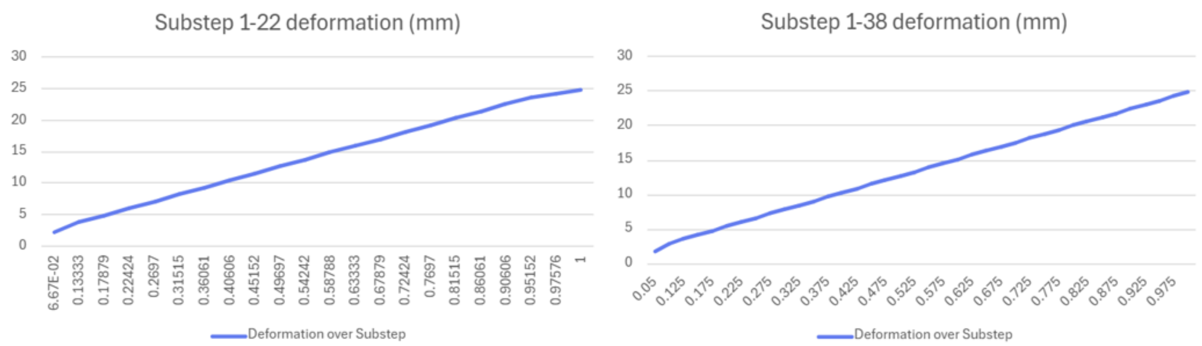

Figure 24: Deformation per substep over the function of time

Increasing the amount of substep would furthermore stabilize the equilibrium iterations for each substep. The first substep is always the most unstable. In this case with bending simulation, the force convergence is the most problematic. The calculated residual force must be lower than the force criterion in order to move on into the next substep. The solver will start with a high residual value and decrease to the criteria value. Sometimes the residual value might increase, which will visualize peaks which in turn will affect the time consumption for reaching the criteria value. Figure 25 visualizes the number of iterations between the residual and criteria force over the first substep. One is the first of 22 substep and the other is the first of 38 substep. The less peaks, the more stable the solution will become.

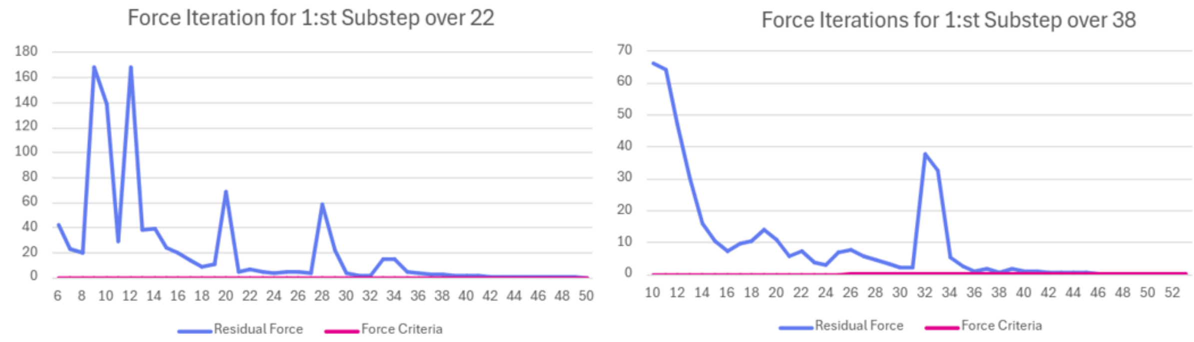

Figure 25: Force convergence iteration process over 1st substep

Large deflection is an option that accounts for changes in stiffness due to changes in shape. This option is typically recommended for nonlinear solutions that include nonlinear material property, large strain in relation to stress like rubber material, or nonlinear contacts like friction or frictionless [39]. Using the large deflection option would make the equilibrium iterations smoother for it to reach the criteria value. This study did not always utilize the option due to the difference between the results being very small. The time-consumption between simulations with and without large deflection option on was not noticeable either. However, the possibilities for higher accuracy are greater for large deformation which was sometimes noticeable from this study's results. The Ansys software would furthermore recommend this option.

Figure 25 shows the residual, and criteria force over approximately 50 equilibrium iterations. The default number of iterations is between 15 to 26, depending on what kind of load the model is affected by [40]. Many simulations during the study needed more iterations than 26 which required the command to override the number of iterations. The command "NEQIT, number" lets the solver utilize the max number of iterations per Substep [40]. Some simulations during the study have reached iterations up to 180, which resulted in the command to be "NEQIT, 200". The command lets the solver, in this case, utilize 200 iterations per Substep. In the case of combining tension and bending in one simulation, the iterative process was either unstable or very time consuming. Even if the number of max iterations were increased from 200 to 400, the calculated residual force would never reach the criteria force in order to converge and move on to next Substep.

5. Conclusion

Over the journey through preparations, execution and analysis, this study evaluates key attributes, limitations and recommendations for future studies with support for a deep understanding of developing a foundation. A foundation which is to improve a physical object by using a complex 3D-model in digital environment, like a power cable in a marine environment.

By combining thermal and mechanical analysis, this study provided a good understanding of how the cable will perform under real marine conditions. The analysis showed how heat generation and dissipation interact with bending and tensile loads and that both effects must be considered. Both thermal stability and mechanical strength are needed to have long-term reliability. The results confirm that the modeling approach is valid and gives ideas for other improvements in material selection, geometry, and simulation methods, which are steps to design cables that can survive some of the most demanding environments on the planet i.e. the sea.

Overall, this study highlights the importance of analyzing both thermal and mechanical behavior in a coupled simulation. The internal heat generation and temperature distribution aren't just thermal issues, they affect how the cable responds to mechanical loads, how materials degrade over time, and how reliable the cable will be in the real world. Proper friction modeling would further improve the accuracy of these predictions, helping to ensure the cable is safe, flexible, and strong enough to withstand the demands of offshore energy systems.

The steps made in this study to research cables in digital environments for the goals of safety, reliability and durability, are moderately successful but have given many insights of consideration. The main steps performed were the thermal behavior and the method of replicating fiber components in FEA. Further steps to accurately combine thermal and mechanical analysis, understandings for stress and fatigue, are proposed for future studies of cables in digital environments.

By improving subsea cable reliability and efficiency, this work supports the transition to clean energy and aligns with and UN SDG 13 [5] and SDG 7 [6].

5.1 Summary of Work

The thermal modelling in this thesis provides a consistent and reliable picture of how a marine power cable behaves under electrical loading. The analysis was carried out step by step, beginning with the representation of electrical losses as heat generation in the conductor. This approach ensured that the simulations were firmly based on physical principles, where current flow is translated into internal heating and then transported through the different material layers of the cable.

A key aspect of the methodology was the treatment of external cooling. Instead of assuming a fixed convection coefficient, the heat transfer to seawater was derived from well-established correlations. This made the model sensitive to the properties of the marine environment, such as temperature and fluid behavior, and gave credibility to the prediction of how the cable interacts with its surroundings. In this respect, the work follows the same scientific reasoning as recent studies in the field, where convection is recognized as the most decisive factor for cable temperature.

The staged simulations, i.e. electro-thermal, steady-state thermal, and transient thermal, all pointed towards the same outcome. They showed a clear radial temperature gradient from the conductor, through the insulation and structural layers, to the cooled outer surface. The transient simulations further demonstrated that the system heats up in a stable and predictable manner, with no sudden jumps or instabilities, before reaching an equilibrium. In conclusion, the transient thermal analysis confirmed that the cable stabilizes at a safe temperature of 36,689 °C after about 58 minutes (3500 seconds) of operation, reinforcing its thermal reliability and suitability for long-term underwater use. This consistency across different modelling steps confirms that the chosen setup is robust.

From a design perspective, the results indicate that the cable remains well within safe thermal limits. The predicted temperatures are far below the maximum operating values for the insulation and protective layers, meaning that the thermal loading under the studied conditions does not pose a risk of overheating. Instead, the analysis suggests that the cable operates with a comfortable thermal margin.

Overall, the conclusions drawn here show that the modelling chain, the electrical heating, conduction through the layers, and convection to seawater, have been correctly implemented. The method is physically well-founded, agrees with practices reported in the literature, and delivers results that can be trusted to represent realistic operating behavior of submarine power cables.

The mechanical analysis was a good initial beginning of a reliable foundation that went through multiple preparations and understanding in its iterative solving process and methods. Firstly, by identifying the specific materials that were used for the experiment hosted by Chalmers. Furthermore, the effective material properties for the materials that were constructed as fiber components. The transformation for these effective material properties is not finalized for accurate fiber behavior. The deformation was furthermore the central point, rather than stress, fatigue and thermal attributes.

The focus on the conductors gave a deeper understanding in the process of iterative solving methods with different model settings for the contacts, mesh and local coordinate systems. It gave furthermore a deep understanding in general settings like manually set substeps, large deflection, the use of stiffness matrix with Newton-Raphson method and commands to override hidden default settings. The solver was not as successful as combining multiple loads, like combining tension and bending simultaneously, and thereby receiving a converged solution. It was therefore more effective to utilize one kind of load per simulation to receive successful solutions.

5.2 Key Findings

The mechanical analyses had many findings in their solving behavior while changing the settings for a stable solution. The fact that the contacts made the solution model nonlinear, the solving process had to use Newton-Raphson's iterative solving method. The solver made iterations of equilibrium calculations through multiple stress factors like displacement, force and moment which all needed to reach a certain criterion in order to converge. Focusing on settings like stiffness matrix structure, large deflection, mesh resolution, brick integration and contact formulations. The solution could be affected positively by valid accuracy and less time-consumption. It is important to note that much of the solution's process is determined by the computer's power properties like processor and random-access memory. The more power, the faster the solution is solved, which is not available for average computer users.

The beam method to replicate the experimental cable is the better alternative for accurate replication. With moments of inertia only to consider balancing the right stiffness while bending and elasticity to consider for tension. However, the beam method could result in more solution instability which was noted by the significant difference in time consumption.

This resulted in more consideration of the right solver settings. Furthermore, utilizing the Contact tool was a great method to analyze a preview of any contact statuses.

Furthermore, key findings for the thermal analysis are that the thermal simulations (thermal-electric, steady-state, and transient) showed that the cable maintains safe operating temperatures under electrical load, with conductor temperatures staying below 38 °C well within the XLPE insulation limit. Heat dissipation through convection to seawater was effectively modeled using Rayleigh–Nusselt correlations, resulting in a realistic convective heat transfer coefficient (~485 $W/m^2 \cdot °C$).

The transient simulation revealed that the cable reaches thermal equilibrium after approximately 58 minutes (3500 seconds), indicating stable thermal behavior during startup. Finally, a clear radial temperature gradient was observed across the cable layers (copper, XLPE, Kevlar, TPU), confirming the importance of material selection and layer thickness in thermal performance.

5.3 Limitations

Solutions with user-defined variables never displayed any stress data. Bending stress and equivalent stress were not possible to examine on the fiber components with reduced moment of inertia, as it was categorized as user-defined variable. The stress and strain data was however saved in the "Solution Coordinate System" according to warning messages after simulated solutions. After analyzing solution information, it was unknown if it is accessible for the user to retrieve the data. There were limitations on tutorials and support guides to access the data.

The seawater temperature was assumed to be 2°C, which may not reflect real-world variations. This simplification could affect the accuracy of thermal safety margins. Radiative heat loss was considered negligible, which is valid at low temperatures but may cause less accuracy in high-current or warmer environments. Electrical resistivity changes with temperature were not fully integrated into the simulation, potentially underestimating heat generation in prolonged high-load scenarios.

The helically winded copper conductor was modeled as a solid cylinder, which improves computational efficiency but may overlook fiber-level heat distribution nuances. Some thermal boundary parameters were repeated across sections, which could be streamlined or clarified for better readability and traceability.

Stress analysis was not performed in detail in this study. The mechanical simulations focused on deflection (bending and tension) to replicate experimental behavior and compare stiffness among conductor models. Comprehensive stress evaluation (e.g., yield, compressive, fatigue) is proposed for future work. Fully coupled bending and tension cases were furthermore not run. Only single-load cases were analyzed. Coupled cases are planned for future work to assess interaction effects.

5.4 Recommendations for Future Work

It is recommended to research further in transforming a solid material property to its effective material that behave like a fiber component in a straight direction and helical winding. A combination of beam models and finalized material property transformation could be interesting to delve into. This is because tempering both elasticity and moment of inertia could provide better tension and bending relations instead of determining one each in separate simulation. The moment of inertia dominates bending behavior while elasticity dominates tension behavior. Using both methods in a valid course of action is interesting for receiving a valid replication of the experimented marine cable that was hosted by Chalmers. If stress and fatigue are of interest in future studies, then more research is needed in transforming a solid material into a fiber component. This study delved into only changing the elasticity and moment of inertia which mainly affects deformation, while some were delved into stress limitations for yield and compression strength. However, more research is needed for transverse stress and fatigue limitations which would complete the Hooke's law that regards elongation, stress and elasticity matrices. Furthermore, if stress and fatigue are of interest in simulated solution with user-defined variables. More research is needed on how to access the stress data that is stored in the "Solution Coordinate System" and display them in the result data.

Future models could incorporate seasonal, regional or depth seawater temperature variations to better reflect real-world operating conditions. Consider also including radiative heat loss for high-current applications and warmer environments to ensure comprehensive thermal modeling. To better predict the Joule heating under varying thermal loads it would be good to integrate dynamic electrical resistivity into the simulation. Using fiber-level modeling to better capture internal heat distribution and potential hotspots may also be a way to improve the simulation.

Combining thermal simulation with mechanical simulation is an interesting study to delve deeper into. Some works were partially made in this study. The steady-state thermal result can be fused with a static-structural simulation. Steady-state thermal will therefore include internal stress and thermal elasticity in its results. Steady-state thermal, however, is more thorough with solid 3D-elements and bonded contact status for distributing heat throughout the model. The more successful beam method utilizes one-dimensional mesh distribution, following a more unrealistic combination. The most promising method was to instead implement the average temperature for each component from the steady-state thermal results into the static-structural analysis. This however did not display any heat distribution. If combination of both is of interest in future studies, then more research is needed for realistic analysis, especially in thermal conductivity between each contact with friction or frictionless status. This includes furthermore the thermal elasticity in all materials. Only Copper and XLPE had available data of elasticity over different temperatures in Ansys Granta Edupack software.

One of the most important aspects of this project, from a mechanical perspective, was how to handle friction in the simulation. Although it might seem like a small detail, the friction coefficient most likely has a huge impact on how internal components of the cable interact under load. In a real cable, the copper wires, Kevlar layers, and TPU jacket are all in contact with each other, and they don't just slide freely, there is resistance to motion. That resistance plays a key role in how the cable behaves when bent, stretched, or twisted. What was investigated is that adjusting the friction coefficient might significantly change the way forces are transmitted through the cable. When friction is too low, the internal layers slip too easily. That would make the cable appear more flexible in the simulation, but it also would lead to unrealistic deformation patterns and could underestimate stress in critical areas. On the other hand, if the friction is too high, the fibers would lock together too much. This would make the cable seem stiffer and could increase localized stress, especially where bending or torsion is involved. Thus, choosing the right friction values isn't just a technical detail — it's essential for getting realistic simulation results. A recommendation is to research individual materials and determine a valid and accurate friction coefficient on different materials, before implementing them in FEM analysis. Comparing with what was decided from section 2,5 which is mostly assumed with support from reference, a more accurate coefficients would further reach the goal of accuracy. Friction coefficients could be used to calculate an effective moment of inertia in fiber components. This case could lead to a foundation of transforming an area moment of inertia into an effective area moment of inertia.

6. References

[1] P. Webb, "Introduction to oceanography," *Roger Williams University*, vol. 985, 2021.

[2] A. Ma, M. Zheng, S. Zhang, and T. Qin, "Thermal circuit model of DC submarine cable considering the influence of seawater property variations," *Electric Power Systems Research*, vol. 230, p. 110268, 2024.

[3] M. Á. González-Cagigal, J. C. del-Pino-López, A. Bachiller-Soler, P. Cruz-Romero, and J. A. Rosendo-Macías, "A thermal model for three-core armored submarine cables based on distributed temperature sensing," *Energies*, vol. 14, no. 13, p. 3897, 2021.

[4] J. C. Del-Pino-López and P. Cruz-Romero, "A 3D parametric thermal analysis of submarine three-core power cables," *Proceedings of the Renewable Energy and Power Quality Journal (ICREPQ'20), Granada, Spain,* pp. 2–4, 2020.

[5] Department of Economic and Social Affairs. "Goal 13: Climate Action." *United Nations*. https://globalgoals.org/goals/13-climate-action/ (accessed Jan 7, 2026).

[6] Department of Economic and Social Affairs. "Goal 7 Affordable and Clean Energy." *United Nations*. https://globalgoals.org/goals/7-affordable-and-clean-energy/ (accessed Jan 7, 2026).

[7] J. W. Ringsberg, L. Dieng, Z. Li, and I. Hagman, "Characterization of the mechanical properties of low stiffness marine power cables through tension, bending, torsion, and fatigue testing," *Journal of Marine Science and Engineering*, vol. 11, no. 9, p. 1791, 2023.

[8] J. W. Ringsberg, J. Heidinger, H. Siran, B. Hamilton, and Z. Li, "Influence on the Mechanical Characteristics of Dynamic Power Cable From Internal Temperature Fluctuations Caused by Power Transmission," in *International Conference on Offshore Mechanics and Arctic Engineering*, 2025, vol. 88919: American Society of Mechanical Engineers, p. V002T04A018.

[9] R. Elleuch, K. Elleuch, B. Salah, and H. Zahouani, "Tribological behavior of thermoplastic polyurethane elastomers," *Materials & design*, vol. 28, no. 3, pp. 824–830, 2007.

[10] S. Sato *et al.*, "Dry sliding friction and Wear behavior of thermoplastic polyurethane against abrasive paper," *Biotribology*, vol. 23, p. 100130, 2020.

[11] A. Talapatra and D. Datta, "Experimental and molecular dynamics simulation based investigation to understand tribological performance of graphene reinforced thermoplastic polyurethane (Gr/TPU) nanocomposites," *Tribology International*, vol. 196, p. 109703, 2024.

[12] B. Pinedo, M. Hadfield, I. Tzanakis, M. Conte, and M. Anand, "Thermal analysis and tribological investigation on TPU and NBR elastomers applied to sealing applications," *Tribology International*, vol. 127, pp. 24–36, 2018.

[13] R. Noori. "What Materials Are Fiber Optic Cables Made Of." *The Network Installers Blog*. https://thenetworkinstallers.com/blog/what-materials-are-fiber-optic-cables-made-of/ (accessed Oct 2, 2025).

[14] *Granta EduPack R1*. (2024). Ansys, Inc. [Online]. Available: https://www.ansys.com/products/materials/granta-edupack#tab1-1

[15] Y. Luo, "Improved Voigt and Reuss formulas with the Poisson effect," *Materials*, vol. 15, no. 16, p. 5656, 2022.

[16] R. M. Jones, *Mechanics of composite materials*. CRC press, 2018.

[17] I. M. Daniel, O. Ishai, I. M. Daniel, and I. Daniel, *Engineering mechanics of composite materials*. Oxford university press New York, 1994.

[18] E. Weisstein. "Circle Packing." *Wolfram Mathworld*. https://mathworld.wolfram.com/CirclePacking.html (accessed Oct 2, 2025).

[19] J. Voglar and A. Peperko, "Calculating the sequences behind a hexagonal lattice based equal circle packing in the Euclidian plane," *arXiv preprint arXiv:2403.10530*, 2024.

[20] *European Cable Stranding*, S. A. B. B. GmbH and K. G. Co, Viersen, Germany. [Online]. Available: https://www.sab-cable.com/cables-wires-harnessing-temperature-measurement/technical-data/cables-and-wires/european-cable-stranding.html

[21] H. Hu, J. Yan, S. Sævik, N. Ye, Q. Lu, and Y. Bu, "Nonlinear bending behavior of a multilayer copper conductor in a dynamic power cable," *Ocean Engineering*, vol. 250, p. 110831, 2022.

[22] K. Björk, *Formler och tabeller för mekanisk konstruktion*. Karl Björks förlag (in Swedish), 2017.

[23] RoyMech. "Coefficients Of Friction." https://roymech.org/Useful_Tables/Tribology/co_of_frict.html (accessed Apr 10, 2025).

[24] M. A. Spalding, D. E. Kirkpatrick, and K. S. Hyun, "Coefficients of dynamic friction for low density polyethylene," *Polymer Engineering & Science*, vol. 33, no. 7, pp. 423–430, 1993.

[25] G. West and J. Senior, "Frictional properties of polyethylene," *Wear*, vol. 19, no. 1, pp. 37–52, 1972.

[26] D. Tan, R. Li, X. Yang, Q. He, and H. Gao, "Tribological behavior of PTFE/Kevlar fabric under different contact stresses," *AIP Advances*, vol. 11, no. 3, 2021.

[27] Ansys Inc, "Numerical Modeling of Contact," Presentations slides, 2020.

[28] Ansys Inc, "Contact Theory in Mechanical Analysis," in "Ansys Mechanical User's Guide." Accessed: 2025-10-17. [Online]. Available: https://ansyshelp.ansys.com/public/account/secured?returnurl=/Views/Secured/corp/v251/en/wb_sim/ds_contact_theory.html

[29] S. Lopez. "Contact Modeling in Ansys Mechanical for Beginners." *Ozen Engineering Blog*. https://blog.ozeninc.com/resources/understanding-contacts-in-ansys-mechanical (accessed Oct 17, 2025).

[30] Ansys Inc, "Contact Formulations in Large Deflection Analysis (Advanced)," in "Ansys Mechanical User's Guide." Accessed: 2025-10-17. [Online]. Available: https://ansyshelp.ansys.com/public/account/secured?returnurl=/Views/Secured/corp/v242/en/wb_sim/ds_Contact_Advanced.html

[31] Ö. Sunar. "Advanced Contacts in Ansys Workbench-1." *MECHEAD*. https://www.mechead.com/advanced-contacts-in-ansys-workbench-1/ (accessed Oct 17, 2025).

[32] Ansys Innovation Space. "Newton-Raphson Method -- Lesson 3." *Ansys Inc*. https://innovationspace.ansys.com/courses/courses/computational-resource-considerations-recommended/lessons/newton-raphson-method-lesson-3/ (accessed Sep 15, 2025).

[33] K. Clement, "Choosing Contact Types in Ansys Mechanical," Diversified Relay Diagnostics, LLC, Presentations slides, Aug 8, 2024.

[34] Ansys Innovation Space. "Convergence Trend with Unsymmetric Newton Raphson." *Ansys Inc*. https://innovationspace.ansys.com/courses/courses/topics-in-hyperelastic-material-model/lessons/convergence-trend-with-unsymmetric-newton-raphson/ (accessed Sep 15, 2025).

[35] Ansys Inc, "SOLID186 3D 20-Node Structural Solid Element Description," in "Ansys Element Reference Guide." Accessed: 2025-09-15. [Online]. Available:

https://ansyshelp.ansys.com/public/Views/Secured/corp/v251/en/ans_elem/Hlp_E_SOLID186.html

[36] Ansys Inc, "Integration Schemes in Mechanical Geometry," in "Ansys Mechanical User's Guide." Accessed: 2025-05-08. [Online]. Available: https://ansyshelp.ansys.com/public/account/secured?returnurl=/Views/Secured/corp/v242/en/wb_sim/ds_integration_schemes.html

[37] Ansys Inc, "Continuum Stress Elements Overview," in "Ansys Element Reference Guide." Accessed: 2025-09-15. [Online]. Available: https://ansyshelp.ansys.com/public/account/secured?returnurl=//Views/Secured/corp/v251/en/ans_elem/Hlp_E_continuumelems.html

[38] V. Menon. "Finite Element Analysis — Hourglass effect due to Reduced Integration points." *MEDIUM*. https://medium.com/@vishwajeethareesh.m/finite-element-analysis-hourglass-effect-due-to-reduced-integration-points-35bb54e8b3cf (accessed Sep 15, 2025).

[39] Ö. Sunar. "What is Large Deflection in Ansys?" *MECHEAD*. https://www.mechead.com/what-is-large-deflection-in-ansys/ (accessed Sep 19, 2025).

[40] Ansys Innovation Space. "Dealing with Bisections in Large Deflection Analysis." *Ansys Inc*. https://innovationspace.ansys.com/courses/courses/topics-in-large-deflection-analysis/lessons/dealing-bisections-in-large-deflection-analysis/ (accessed Sep 19, 2025).

7. **Appendix**

Appendix A:

Numerical solution of volume mixture between Kevlar 29 & 49 (Python script)

```
E29 = 71
E49 = 130
v49=1
v29=0

while(True):
    E=(v29*E29)+(v49*E49)
    print(E)
    if (E<=110.00001) & (E>=109.99999):
        break
    v29=v29+0.000001
    v49=v49-0.000001
```

Appendix B:

Solution for Helical winded elasticity matrix in copper and tested with Kevlar (Python script)

```
import numpy as np


#Ef = 110000000000 #Kevlar 29 & 49 (Granta Edupack and Rule of Mixture)
Ef = 126000000000 #Copper (Granta Edupack)
Vf = 0.907 #Kevlar 29 & 49 volume factor
#Vf = 0.9145 #Copper volume factor
#Gf = 1150000000 #Kevlar 29 & 49 (Granta Edupack and Rule of Mixture)
Gf = 46840000000 #Copper (Granta Edupack)
E11 = E22 = E33 = Ef*Vf
G12 = G13 = G23 = Gf*Vf

S11 = 1/E11
S12 = -v12/E11
S22 = 1/E22
S66 = 1/G12
theta = np.pi/18

S11prime = (S11*(np.cos(theta)**4)) + (((2*S12)+S66)*(np.sin(theta)**2)*(np.cos(theta)**2)) +
(S22*(np.sin(theta)**4))
S12prime = (S12*((np.sin(theta)**4)+(np.cos(theta)**4)))+((S11+S22-
S66)*(np.sin(theta)**2)*(np.cos(theta)**2))
S22prime = (S11*(np.sin(theta)**4)) + (((2*S12)+S66)*(np.sin(theta)**2)*(np.cos(theta)**2)) +
(S22*(np.cos(theta)**4))
S66prime = (2*((2*S11)+(2*S22)-(4*S12)-S66)*(np.sin(theta)**2)*(np.cos(theta)**2)) +
(S66*((np.sin(theta)**4)+(np.cos(theta)**4)))

E11prime = 1/S11prime
E22prime = E33prime = 1/S22prime
G12prime = G13prime = 1/S66prime
v12prime = v13prime = E11prime*S12prime
v23prime = (E22prime/(2*G23))-1
G23prime = G23
```

Appendix C:

Hexagonal generating fiber layout

```
import numpy as np

import matplotlib.pyplot as plt


D_bundle_new = 6.4  # Total diameter of Kevlar component

#D_bundle_new = 9.3  # Total diameter of Copper fiber conductor

R_bundle_new = D_bundle_new/2 # Radius of fiber component

d_fiber_new = 0.015 # Diameter of individual aramid fiber

#d_fiber_new = 0.031 # Diameter of individual copper fiber

A_fiber_new = np.pi*((d_fiber_new/2)**2) # Area of individual aramid fiber


# Vertical and horizontal spacing for new fibers

row_spacing_new = d_fiber_new*np.sqrt(3)/2

col_spacing_new = d_fiber_new


# Estimate number of rows and columns needed

num_rows_new = int(R_bundle_new/row_spacing_new)+1

num_cols_new = int(R_bundle_new/(0.5*d_fiber_new))+1


# Generate hexagonal grid for new configuration

hex_positions_new = []

for row in range(-num_rows_new, (num_rows_new+1)):

    y = row*row_spacing_new

    for col in range(-num_cols_new, (num_cols_new+1)):

        if (row%2) == 0:

            x_offset = 0

        else:

            x_offset = 0.5*d_fiber_new


        x = (col + x_offset / d_fiber_new)*col_spacing_new

        if (x**2 + y**2) <= (R_bundle_new**2):

            hex_positions_new.append((x, y))
```

```
# Compute area moment of inertia with transfer formula
I_hex_new = 0
for _, y in hex_positions_new:
    I_hex_new += A_fiber_new * y**2

n_fibers_hex_new = len(hex_positions_new) # Number of fibers in the component
A_total_hex_new = n_fibers_hex_new*A_fiber_new # Area consued by fibers

# Plotting the new hexagonal layout
x_hex_new, y_hex_new = zip(*hex_positions_new)
plt.figure(figsize=(6, 6))
plt.scatter(x_hex_new, y_hex_new, s=1, color='purple', label='Fiber centers (new)')
circle_new = plt.Circle((0, 0), R_bundle_new, color='r', fill=False, linestyle='--', label='Bundle boundary')
plt.gca().add_patch(circle_new)

plt.title("Hexagonal Fiber Packing Kevlar = 0,907") # Title for Kevlar component layout
#plt.title("Hexagonal Fiber Packing Copper = 0,9145") # Title for Copper fiber layout
plt.xlabel("x (mm)")
plt.ylabel("y (mm)")
plt.axis('equal')
plt.grid(True)
plt.legend()
plt.show()

# Volume packing in different execusion
volume_1 = (n_fibers_hex_new*(np.pi*(d_fiber_new/2)**2))/(np.pi*(D_bundle_new/2)**2)
volume_2 = A_total_hex_new/(np.pi*(R_bundle_new**2))
```

Appendix D:

Displacement conditions for bending

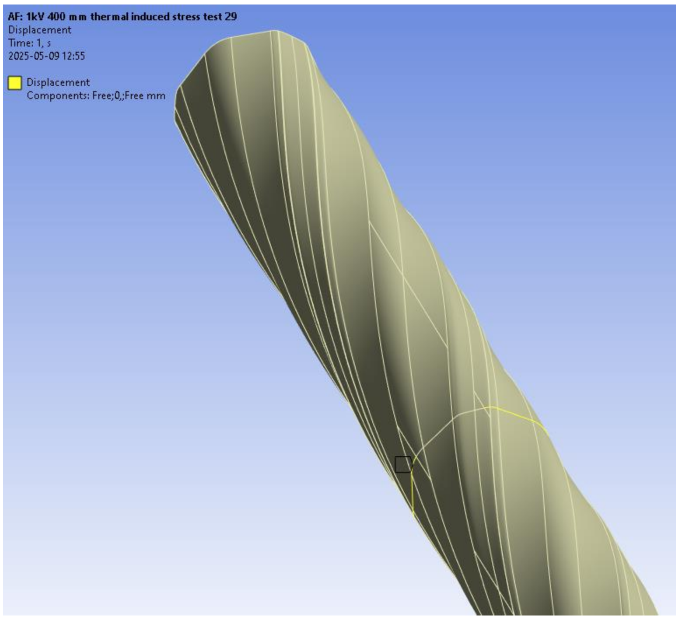

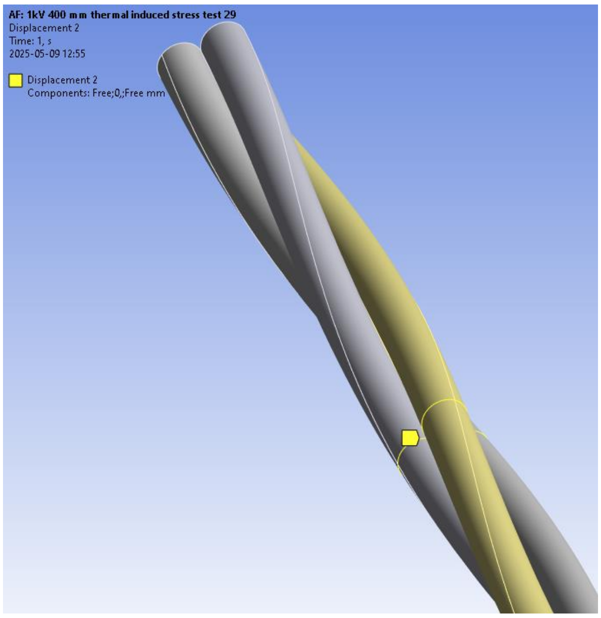

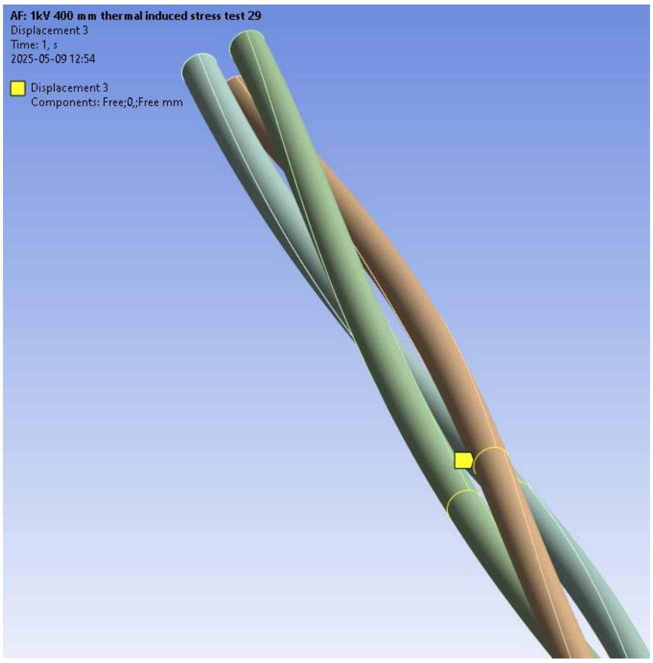
AF: 1kV 400 mm thermal induced stress test 29
Displacement 3
Time: 1, s
2025-05-09 12:54
Displacement 3
Components: Free;0,;Free mm

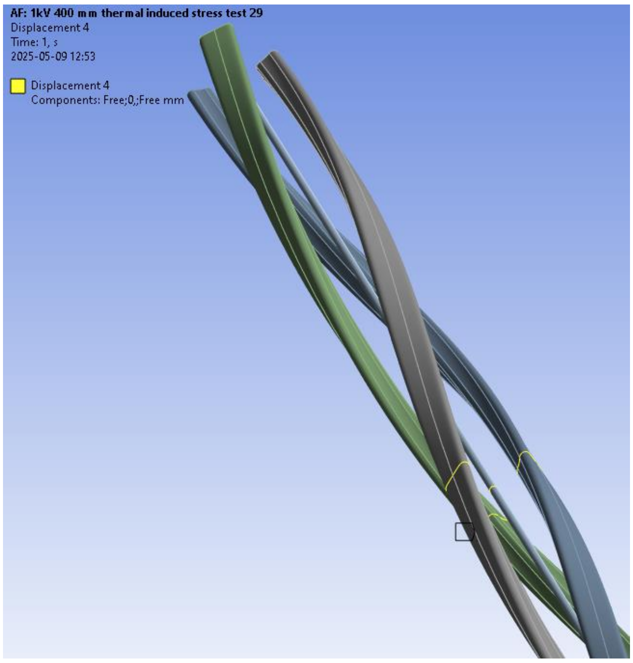
AF: 1kV 400 mm thermal induced stress test 29
Displacement 4
Time: 1, s
2025-05-09 12:53
Displacement 4
Components: Free;0,;Free mm

Appendix E:

Displacement conditions for tension

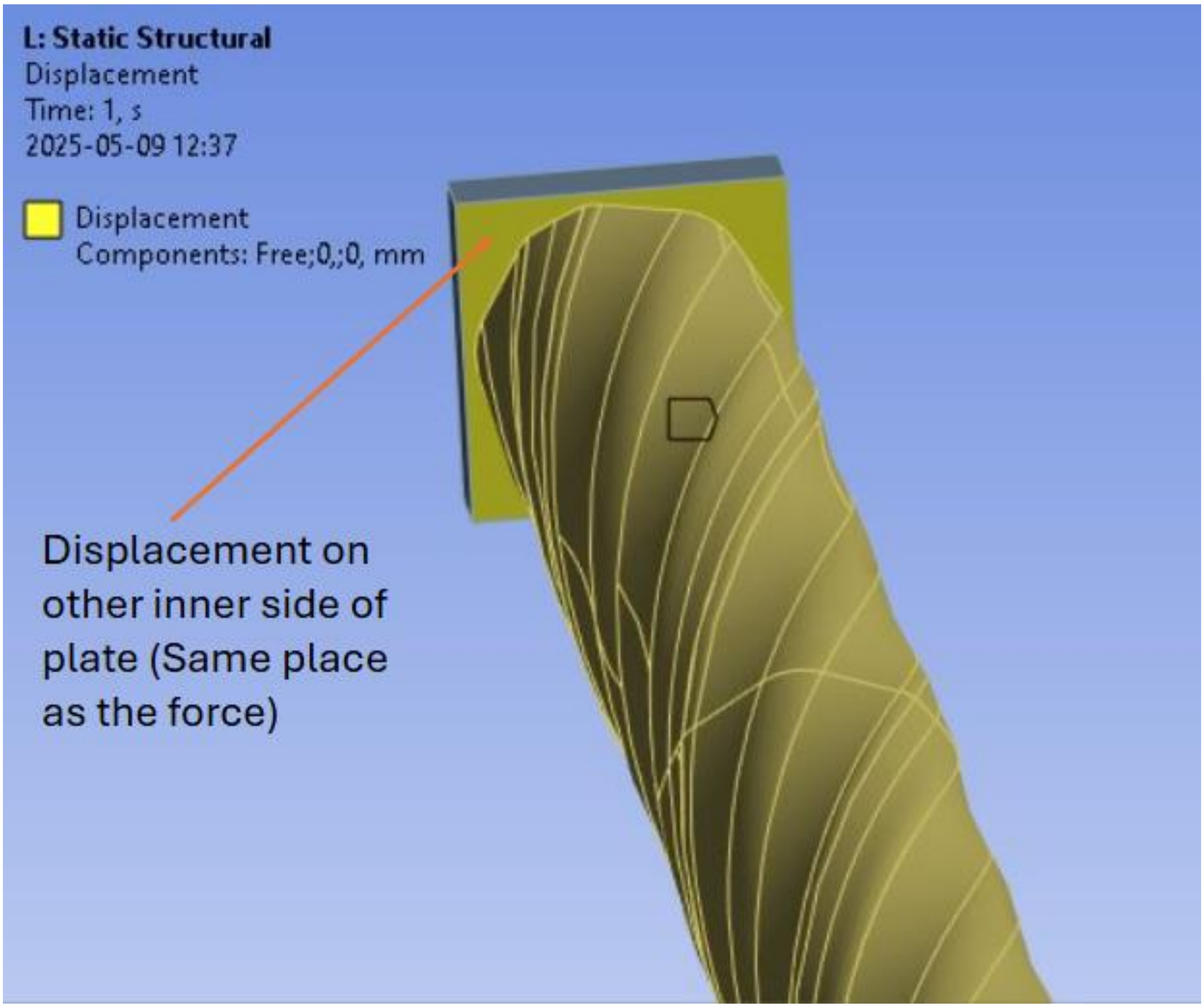

Appendix F:

Thermal-static results with average temperature applied

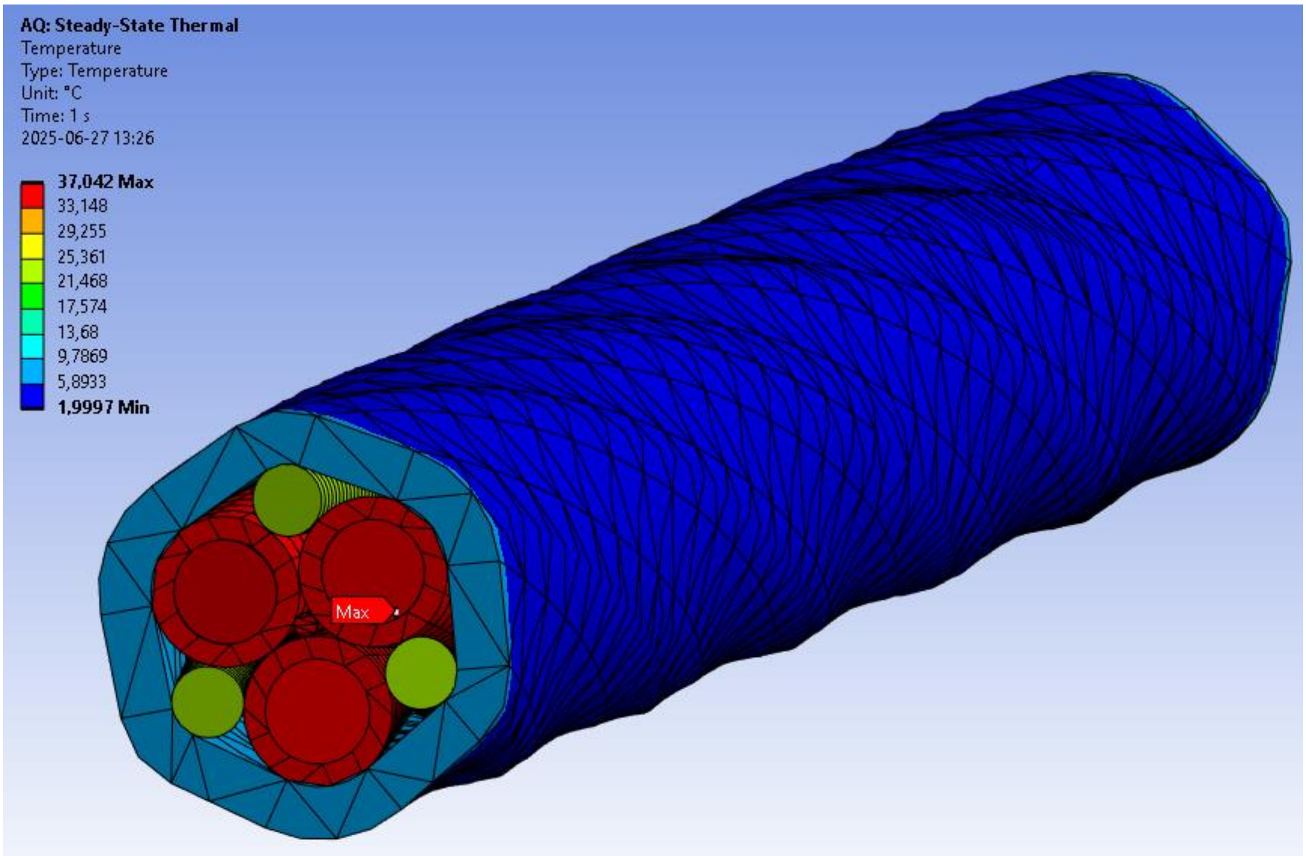

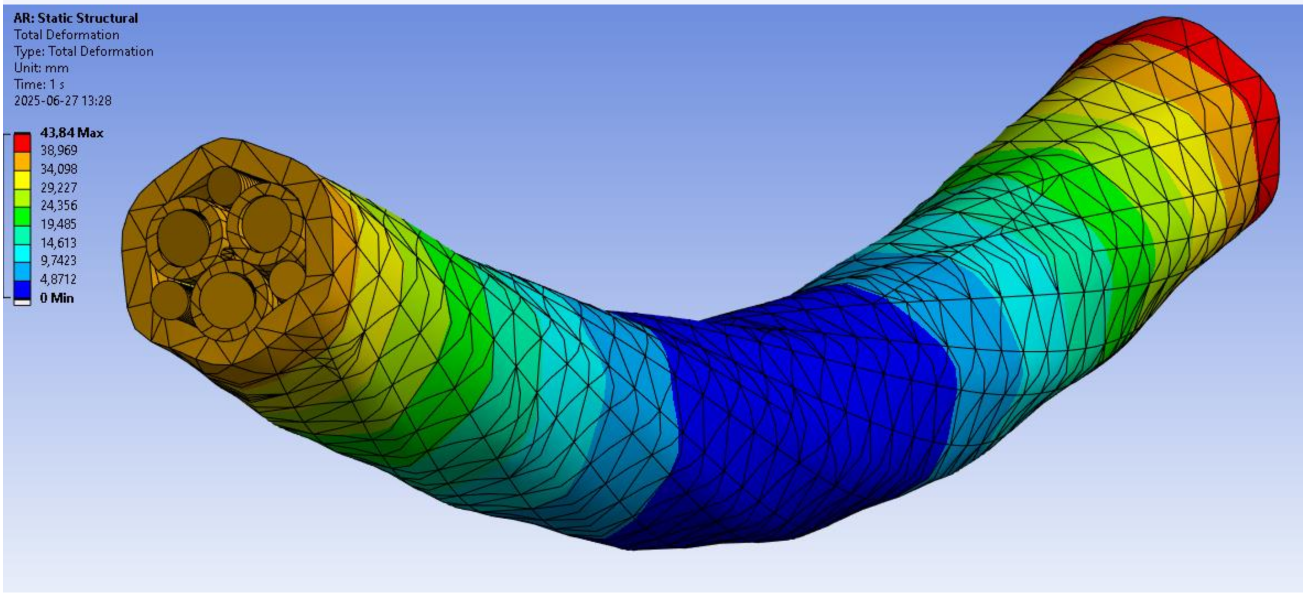

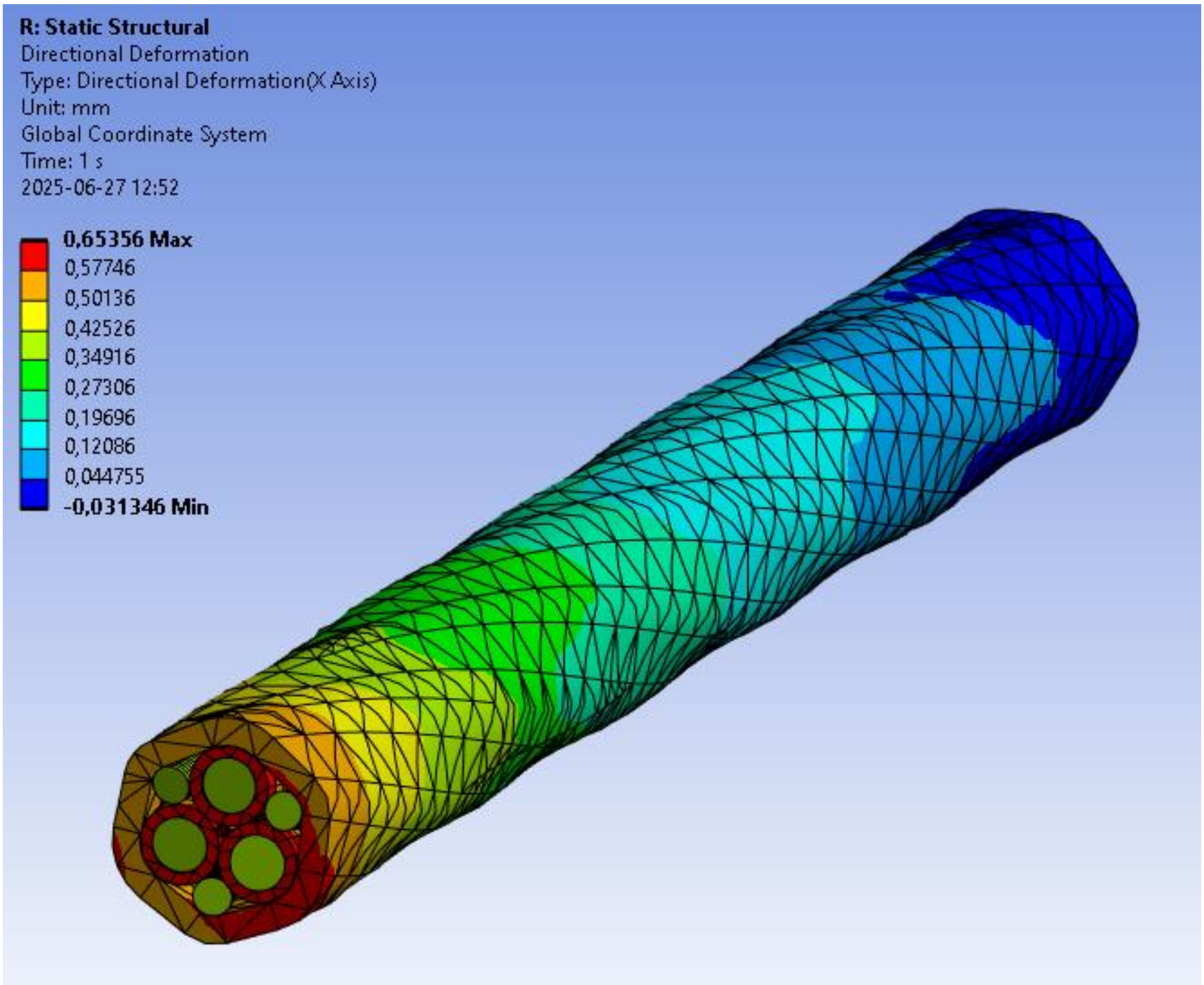
R: Static Structural
Directional Deformation
Type: Directional Deformation(X Axis)
Unit: mm
Global Coordinate System
Time: 1 s
2025-06-27 12:52
0,65356 Max
0,57746
0,50136
0,42526
0,34916
0,27306
0,19696
0,12086
0,044755
-0,031346 Min

INSTITUTIONEN FÖR
MEKANIK OCH MARITIMA VETENSKAPER
CHALMERS TEKNISKA HÖGSKOLA
Göteborg, Sverige 20xx
www.chalmers.se

CHALMERS